https://doi.org/10.5194/egusphere-2025-4590
Preprint. Discussion started: 6 January 2026

Exploring the applicability of Censored Shifted Gamma Distribution (CSGD) error model to radar based rainfall nowcasts: A UK case study

Hung-Ming Lin[1], Li-Pen Wang[1,2], and Jen-Yu Han[1]

[1]Department of Civil Engineering, National Taiwan University, 10617 Taipei, Taiwan
[2]Department of Civil and Environmental Engineering, Imperial College London, SW7 2AZ London, United Kingdom

Correspondence: Li-Pen Wang (lpwang@ntu.edu.tw)

Abstract. Radar based rainfall nowcasting plays a critical role in hydrological operations such as stormwater management and flood early warning. Compared with Numerical Weather Prediction (NWP), it offers higher short-term accuracy and lower computational costs. However, operational uptake remains constrained by two key challenges: (i) uncertainties in nowcasting algorithms and (ii) discrepancies between radar rainfall estimates and ground based measurements. Focusing on the latter, this study explores the potential of the Censored Shifted Gamma Distribution (CSGD) error model to adjust high-resolution radar nowcasts using gauge observations, thus improving their hydrological applicability. The proposed framework involves calibrating both climatological and conditional CSGD models at gauge locations and interpolating parameters across the study area. Deterministic and ensemble nowcasts generated by the Short-Term Ensemble Prediction System (STEPS) are subsequently adjusted using linear and non-linear CSGD models. In this process, predicted rainfall intensities are transformed into cumulative distribution functions (CDFs), enabling probabilistic nowcasting. The median of the CSGD-derived distributions is then applied as the adjusted rainfall intensity, improving alignment with ground observations. Results suggest that combining STEPS ensemble nowcasting with the non-linear CSGD model generally yields the best performance, with error reductions approaching 6% at the 6 h lead time (hourly scale) and at the 3 h lead time (5 min scale) and uncertainty reductions approaching 20% across selected events. These findings demonstrate the potential of extending the CSGD method –originally developed for daily satellite precipitation estimation– to hourly and sub-hourly timescales. This advancement enhances the reliability of radar based predictions and their value for hydrological decision-making.

1 Introduction

Radar based precipitation nowcasting has become an essential tool in operational hydrology, especially for disaster management and early warning applications (Yao et al., 2022; Willems et al., 2017; Ten Veldhuis et al., 2014; Pan et al., 2021). Unlike Numerical Weather Prediction (NWP), radar based nowcasting requires fewer operational resources while providing higher forecast accuracy for short lead times (Imhoff et al., 2023; Radhakrishnan and Chandrasekar, 2020; Osinski and Bouttier, 2018). Over the past two decades, advances in computer vision (CV) and deep learning (DL) have inspired the development of numerous nowcasting techniques based on CV, DL, or combinations of both (Shi et al., 2015, 2017; Ayzel et al., 2019). In

https://doi.org/10.5194/egusphere-2025-4590
Preprint. Discussion started: 6 January 2026

particular, models using emerging DL techniques, such as Generative Adversarial Networks (GANs), have shown potential to outperform operational models like Short-Term Ensemble Prediction System (STEPS) in terms of nowcasting accuracy (Ravuri et al., 2021; Choi and Kim, 2022).

In spite of these advancements, the inherent errors and the challenge of accurately estimating uncertainty in radar based nowcasting continue to limit its reliability for hydrological applications. It is important to distinguish between 'uncertainty' and 'error' as used in this paper. While they are sometimes used interchangeably in the literature, here, 'uncertainty' refers to the expected range within which the true value should lie with a specified confidence level, whereas 'error' denotes the deviation between the estimated and true values (Massari and Maggioni, 2020). These two concepts primarily originate from two sources: the difficulty in accounting for uncertainty in nowcasting models and the differences between radar rainfall (RR) estimates and gauge rainfall (GR) measurements (Dai et al., 2015, 2013).

The first source of uncertainty corresponds to the intrinsic limitations of nowcasting algorithms, which often struggle to explicitly or deterministically model processes like precipitation initiation, growth, and decay –processes that become increasingly important at extended lead times (Lagasio et al., 2022; Poletti et al., 2019). Recent advancements in nowcasting techniques have sought to address these challenges. For example, STEPS employs ensemble methods to represent uncertainty in atmospheric conditions. By introducing stochastic perturbations to both precipitation intensities and motion fields, STEPS generates multiple forecast members, each representing a plausible outcome, thus enabling ensemble nowcasting (Bowler et al., 2006; Pulkkinen et al., 2019).

In parallel, various Artificial Intelligence (AI) based models have been developed to overcome the limitations of traditional nowcasting algorithms (Shi et al., 2015, 2017; Ravuri et al., 2021; Zhang et al., 2023). For example, the Deep Generative Model of Radar (DGMR) utilises a deep generative framework to produce probabilistic forecasts by sampling from learned conditional distributions via latent random vectors (Ravuri et al., 2021). Unlike DGMR, which generates the nowcast sequence as a whole, NowcastNet introduces a separate Evolution Network to sample rainfall variations explicitly associated with the evolution process (Zhang et al., 2023). These AI based approaches have demonstrated promising potential to outperform existing non-AI nowcasting algorithms.

The second source of uncertainty arises from intrinsic limitations of radar systems and the algorithms used for signal processing, Z-R relationships, and rain-gauge calibration (Dai et al., 2018; Kuo et al., 2014; Tahir et al., 2022). Villarini and Krajewski (2010), for example, identified several primary sources of uncertainty in single-polarization radar rainfall estimates, which can generally be classified into those related to quality control (QC) and hardware limitations.

To address these challenges, dual-polarization radar systems have significantly advanced quantitative precipitation estimation (QPE) since the 1990s, mainly by reducing the errors inherent in traditional single-polarization systems (Qiu et al., 2020; Skripniková and Řezáčová, 2019). Dual-polarization radars transmit and receive both horizontally and vertically polarized waves, providing additional polarimetric measurements, such as differential reflectivity (Z_{DR}), differential phase (Φ_{DP}), specific differential phase shift (K_{DP}) and the co-polar correlation coefficient (ρ_{HV}) (Xia et al., 2020; Gou et al., 2018; Li et al., 2022). Incorporating these parameters into advanced models improves the characterisation of drop size distributions (DSD) across different hydrometeor types (e.g., rain, snow, hail) and helps reduce uncertainties and errors in QPE.

https://doi.org/10.5194/egusphere-2025-4590
Preprint. Discussion started: 6 January 2026

Nevertheless, discrepancies between RR estimates and ground based GR measurements persist. These differences are partly due to the fundamentally different measurement mechanisms of radar and gauges (Seo and Krajewski, 2015; Wang et al., 2015), as well as wind-induced errors (Sandford, 2015; Gires et al., 2022). In the literature, these discrepancies are typically lumped as RR–GR differences and are often addressed using statistical models (Germann et al., 2006, 2009; Dai et al., 2015; Maity et al., 2015; Cecinati et al., 2017; Codo and Rico-Ramirez, 2018).

In this study, we specifically address the uncertainty and error in RR estimates for radar based precipitation nowcasting. Previous studies have proposed various approaches to tackle these challenges. For example, Cecinati et al. (2017) applied Kriging with External Drift, showing that integrating multiple data sources can reduce uncertainty, particularly for urban applications. However, for real-time hydrological operations, rain gauges are not always possible to provide real-time corrections due to measurement delays.

Other studies have employed copulas to model the dependence between RR and GR estimates. Maity et al. (2015) used Frank and Plackett copulas to build joint distributions of radar reflectivity and rainfall, improving spatial rainfall estimation. Yet, their method tends to underestimate high-intensity rainfall (> 10 mm/h), leading to conditional bias. Ensemble based methods have also gained attention. Codo and Rico-Ramirez (2018) developed an ensemble rainfall forecasting framework using rain-gauge data to quantify RR residual errors, which was coupled with a hydrodynamic sewer model to examine uncertainty propagation. However, this method focused on uncertainty quantification without directly improving RR accuracy. The REAL (Radar Ensemble generator for the Alps using LU decomposition) model (Germann et al., 2006, 2009) used stochastic perturbations generated via LU decomposition and AR(2) processes to produce rainfall ensembles. While REAL effectively captures spatial and temporal error structures, it focuses on uncertainty representation rather than reducing the magnitude of RR errors.

Similarly, Dai et al. (2015) introduced two noise models, ERF-TN and ERF-EM, within the STEPS framework to generate ensemble nowcasts. ERF-TN perturbs rainfall intensities and advection fields using Gaussian noise, while ERF-EM uses t-Copulas and historical radar-gauge discrepancies. Despite these advances, both schemes focus primarily on uncertainty quantification, with limited capacity to separately model or reduce systematic biases and random errors.

Although these methods have improved uncertainty representation in RR estimates, they remain limited in their ability to reduce errors and uncertainty simultaneously, particularly for short-term forecasting. Recently, statistical postprocessing techniques have emerged as a promising strategy for improving precipitation estimates from satellite datasets (Maggioni et al., 2016; Maggioni and Massari, 2018; Li et al., 2023), NWP models (Scheuerer and Hamill, 2018), and GCMs (Schepen et al., 2017, 2018). These methods model differences between datasets using observed precipitation as a reference and are particularly effective in enhancing accuracy for extreme events, improving spatial interpolation, and maintaining robustness under data gaps or outliers (Mamalakis et al., 2017; Villarini et al., 2022; Xu et al., 2022). For example, Maggioni et al. (2014) proposed the PUSH scheme, a probabilistic framework for estimating satellite precipitation errors, effectively capturing systematic and random errors, missed events, and false alarms. However, PUSH treats hits, misses, and false alarms using separate models, requiring additional parameters and lacking a unified theoretical structure (Wright et al., 2017).

To address these limitations, Wright et al. (2017) introduced the Censored Shifted Gamma Distribution (CSGD) framework, initially developed for satellite precipitation data postprocessing. The CSGD framework integrates a shift parameter (δ) into the

https://doi.org/10.5194/egusphere-2025-4590
Preprint. Discussion started: 6 January 2026

gamma distribution's cumulative distribution function to simultaneously model false alarms, misses, and hits. Two calibration approaches were proposed: climatological CSGD, based on historical reference data (e.g. radar NLDAS-2), and conditional CSGD, based on concurrent satellite and reference data. This framework effectively reduces systematic biases and quantifies uncertainties, showing strong performance across diverse precipitation regimes, including complex terrains. However, the original CSGD framework was calibrated with radar based reference data at daily scales, limiting its spatial and temporal resolution for real-time nowcasting. Radar data often carry their own measurement uncertainties, and the coarse resolution of satellite data further limits its suitability for short-term hydrological forecasting. In addition, the framework does not apply well in regions without reference data.

To overcome these limitations, this study proposes to modify the CSGD framework by using rain-gauge data as the reference and treating RR data as the satellite dataset to model inherent uncertainties. The method is adapted to operate at an hourly (and sub-hourly) scale with 1 km spatial resolution, aligning with the native resolutions of the GR and RR datasets. Given the point based nature of GR observations, the method may initially appear restricted to grids containing rain gauges. To address this, we incorporate parametrisation into the modeling process, conduct spatial structure analysis, and perform parameter interpolation to extend the model's applicability across the radar domain. The results and remaining limitations of this approach are further discussed in later sections.

The rest of the sections of this study is organised as follow. The study area and rainfall data used in this research are detailed in Sect. 2. The methods for calibrating the CSGD models, interpolating CSGD parameters, conducting radar based precipitation nowcasting, and performing evaluations are presented in Sect. 3. The results of CSGD parameter interpolation and adjustments to radar precipitation nowcasting are provided in Sect. 4. A summary and overall discussion are offered in Sect. 5.

2 Study area and data

2.1 Study area

The study area covers a 512 km $\times$ 512 km region centred on Birmingham, UK. Its boundaries are defined by the coordinates (149,000 m, 32,000 m) (approximately $5.51°$W, $50.13°$N) in the lower-left corner and (611,000 m, 544,000 m) (approximately $2.05°$E, $54.72°$N) in the upper-right corner, referenced under the OSGB36 Geodetic Coordinate System and WGS84 datum. The southern UK falls under the Köppen-Geiger climate classification Cfb (Beck et al., 2018), representing a temperate oceanic climate with mild winters and summers and well-distributed precipitation throughout the year.

Snowfall is relatively infrequent in the region, with an average of only 15.6 days per year of snow cover across the UK, and even fewer in the southern areas (Met Office, b). Consequently, rainfall accounts for the vast majority of annual precipitation in the study area. To focus on rainfall nowcasting and avoid the significant undercatch errors in rain-gauge measurements associated with snowfall (Fassnacht, 2004), snowfall events were excluded. This also mitigates biases arising from precipitation phase identification, where similar radar reflectivities can correspond to different precipitation amounts depending on phase (Sims and Liu, 2015).

https://doi.org/10.5194/egusphere-2025-4590
Preprint. Discussion started: 6 January 2026

Annual rainfall varies markedly across the region, from approximately 2,500 mm in the mountainous west to around 500 mm in the eastern lowlands (see Figure 1b), reflecting strong influences of altitude and longitude (see Figure 1a) (Wang et al., 2024). This climatological diversity ensures that the proposed methodology is tested across a wide range of geographical and physiographic conditions.

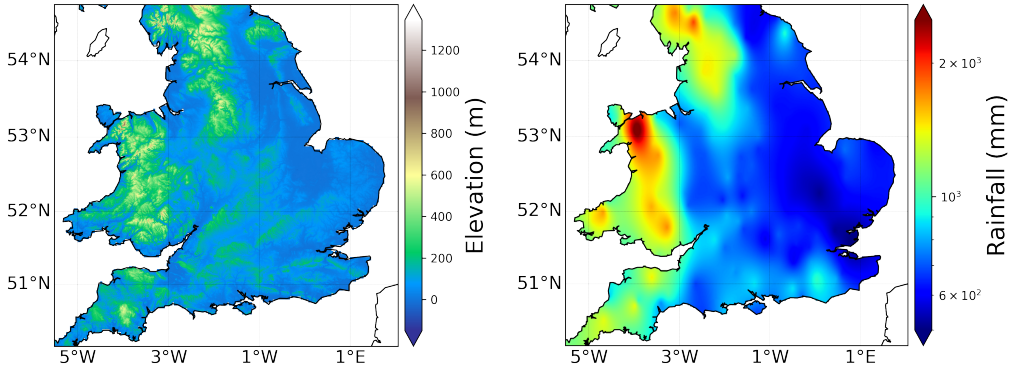

Figure 1. Orographic and climatological overview of the study area: (**a**) terrain elevation (in metre), and (**b**) average annual rainfall (in mm) computed and interpolated from MIDAS data.

2.2 Rainfall data

In this study, the high-quality rain-gauge and radar rainfall datasets, provided by the UK Met Office, are used for model calibration and verification at 1 h timescales in this study. In addition, Environment Agency (EA) gauge records over the Severn Trent catchment (a sub area within the study area) are employed to evaluate the proposed model at the 5 min timescale.

2.2.1 Rain gauge records

The Met Office Integrated Data Archive System (MIDAS) (Met Office, 2019) is a comprehensive database managed by the UK Met Office, containing meteorological observations dating back to 1853. It includes a wide range of weather variables —such as rainfall, humidity, temperature, and wind speed –recorded at temporal resolutions ranging from hourly to daily (Kendon et al., 2022). The MIDAS dataset has been widely utilised in the literature, highlighting its credibility and importance for meteorological research (King et al., 2021; Xi and Sokolik, 2015; McClean et al., 2020).

In this study, we employ 1 h quality-controlled rainfall data from the MIDAS archive. Specifically, the latest version of the MIDAS rainfall dataset, retrieved from the Centre for Environmental Data Analysis (CEDA), covering the years 2016–2022, is used. Following a completeness assessment of station records within the study area and period, a total of 156 stations are selected for model calibration (2016–2020) and verification (2021–2022). The spatial distribution of these stations is illustrated in Figure 2a.

https://doi.org/10.5194/egusphere-2025-4590
Preprint. Discussion started: 6 January 2026

In addition to MIDAS data, a set of Environmental Agency (EA) rain-gauge records at 5 min resolution over the Severn Trent (ST) region –a sub-area within the study domain– is employed for result verification. The EA-ST dataset originally includes 258 stations distributed within approximately a 250 km radius centred on Birmingham. This dataset was recorded in time of tips and was further processed to 5 min resolution to match that of the NIMROD radar dataset. This enables evaluation of radar based nowcasting performance at sub-hourly timescales rather than relying solely on hourly accumulations. A basic quality control was performed by comparing the EA-ST gauge records against nearest MIDAS observations at the 1 h scale. Pearson correlation coefficients were computed, and a total of 103 stations with a coefficient greater than 0.7 were selected for further validation analyses.

2.2.2 Radar data

Developed by the UK Met Office, the Nimrod radar rainfall composite dataset has been available since late 2002, providing 5 min temporal resolution on a 1 km Cartesian grid covering the UK (Golding, 1998; Yu et al., 2020). The Nimrod system applies algorithmic corrections to radar-estimated precipitation intensities, incorporating real-time rain-gauge measurements at hourly intervals to improve data accuracy (Harrison et al., 2000; Kidd et al., 2012).

In this study, Nimrod data from 2016 to 2022 is used, with records from 2016 to 2020 employed for model calibration and those from 2021 to 2022 used for result verification. For each time step, the Nimrod data is spatially cropped to a 512 × 512 pixel square, aligning with the study domain. To ensure consistency with the MIDAS dataset, the original 5 min radar data is aggregated to an hourly timescale for model calibration.

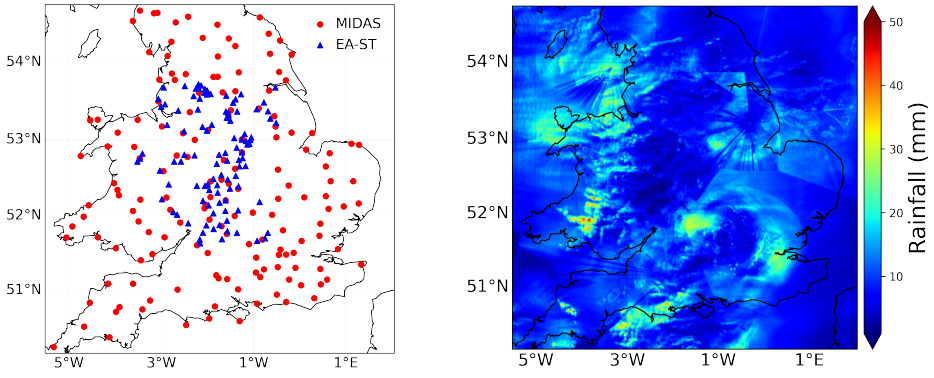

(a) (b)

Figure 2. Rainfall datasets demonstration: (**a**) spatial distribution of MIDAS and EA-ST stations, and (**b**) example rainfall accumulation from the NIMROD radar dataset (case no.1).

2.3 Event selection

For results verification, a total of 20 storm events from 2021 and 2022 were selected based on the following criteria:

https://doi.org/10.5194/egusphere-2025-4590
Preprint. Discussion started: 6 January 2026

1. A given time step is classified as *wet* if more than 10% of the pixels within the study domain register rainfall intensities $\geq$ 1 mm/h; otherwise, it is classified as *dry*.

2. A storm event begins with a *wet* timestamp and continues until a subsequent *dry* period lasting at least 8 hours occurs.

3. A storm event ends at the last *wet* time step preceding a *dry* period of $\geq$ 8 hours.

Applying these criteria resulted in an initial pool of 74 and 67 storm event candidates in 2021 and 2022, respectively. To prioritise events most relevant to hydrological applications, we further filtered events based on their *wet* coverage rate over the land area and overall duration. In addition, we ensured seasonal diversity to include a representative mix of storm types, such as convective and stratiform systems. Eventually, 20 events were selected –10 from each year– with even distribution across seasons. Event start and end times were rounded to the nearest clock hour to align with the hourly resolution of the MIDAS dataset.

Summary statistics for the selected events are provided in Table 1. The correlation coefficients between maximum rainfall accumulations from the MIDAS rain gauges (denoted as GR) and the Nimrod radar estimates (denoted as RR), as well as between their respective mean values, are 0.79 and 0.96, respectively. These results indicate a generally high level of consistency between the two datasets. A spatial plot of accumulated Nimrod rainfall (in mm) for Event 1 across the study domain is presented in Figure 2b.

https://doi.org/10.5194/egusphere-2025-4590
Preprint. Discussion started: 6 January 2026

Table 1. Selected storm Events for result verification and the summary statistics results from MIDAS (GR) and Nimrod (RR), respectively (UTC)

Event	Start time	End time	Duration	Rainfall accumulation (mm)			
				Max.		Mean	
			(hours)	GR	RR	GR	RR
1	2021-01-15 22:00	2021-01-16 18:00	20	26.0	22.9	6.6	10.3
2	2021-03-09 22:00	2021-03-11 00:00	26	81.2	45.4	12.8	12.7
3	2021-05-03 08:00	2021-05-04 05:00	21	63.6	33.6	15.9	13.5
4	2021-05-08 01:00	2021-05-08 21:00	20	52.2	45.9	16.8	13.7
5	2021-05-20 09:00	2021-05-22 02:00	41	107.8	96.5	18.4	18.6
6	2021-05-23 11:00	2021-05-24 07:00	20	29.0	33.5	9.5	9.0
7	2021-07-05 17:00	2021-07-06 13:00	20	29.8	32.8	12.5	11.8
8	2021-10-02 05:00	2021-10-03 02:00	21	37.6	67.8	14.6	13.3
9	2021-10-31 03:00	2021-11-01 07:00	28	53.4	61.0	18.1	16.3
10	2021-12-07 08:00	2021-12-08 05:00	21	38.8	34.4	9.0	9.7
11	2022-01-08 04:00	2022-01-08 22:00	18	29.8	24.4	7.4	8.1
12	2022-03-16 11:00	2022-03-17 05:00	18	27.8	27.5	7.9	8.6
13	2022-04-12 06:00	2022-04-12 19:00	13	13.4	24.4	2.8	3.0
14	2022-05-11 02:00	2022-05-11 20:00	18	22.2	23.6	6.3	6.2
15	2022-05-15 20:00	2022-05-16 11:00	15	19.8	22.7	4.9	5.1
16	2022-06-18 15:00	2022-06-19 06:00	15	18.6	25.3	3.5	4.8
17	2022-08-25 05:00	2022-08-25 19:00	14	34.6	32.5	4.9	5.5
18	2022-09-30 09:00	2022-10-01 03:00	18	51.4	31.7	11.9	10.4
19	2022-10-31 18:00	2022-11-01 12:00	18	32.8	30.9	11.6	11.7
20	2022-11-23 03:00	2022-11-23 19:00	16	21.6	25.4	8.3	8.5

https://doi.org/10.5194/egusphere-2025-4590
Preprint. Discussion started: 6 January 2026

3 Methodology

3.1 Overview

The proposed method comprises two primary steps: Censored Shifted Gamma Distribution (CSGD) model calibration and radar nowcast adjustment. As illustrated in Figure 3, the former involves building pixel-wise CSGD models across the study area by integrating point location based CSGD models with spatial interpolation techniques. The second step then applies these models to adjust radar based rainfall nowcasts –resulting from both deterministic and ensemble nowcasting –in real time.

CSGD model calibration (Figure 3 (left)) begins with calibrating a climatological CSGD model at each gauge location using 1 h MIDAS rain gauge data. Then, a conditional CSGD model is constructed at each rain-gauge location by analysing the differences between rain-gauge data and co-located RR pixel data over the study period. Here, both linear and non-linear versions of the conditional CSGD model are tested. Afterwards, a spatial structure analysis of the CSGD parameters is undertaken, characterising the spatial associations between parameters and enabling parameter field generation via spatial interpolation. This results in pixel-wise CSGD models for the entire study area.

The second step, radar nowcast adjustment (Figure 3 (right)), then applies these pixel-wise CSGD models to nowcasts generated from STEPS, such that the hydrological applicability of radar nowcasts can be improved. Specifically, pySTEPS is used to produce 5 min rainfall forecasts for the next few hours based on original RR rainfall fields (Pulkkinen et al., 2019). Then, at each pixel location, the CSGD model is used to adjust the co-located nowcasts. Here, both deterministic and ensemble STEPS nowcasts are produced and adjusted. This allows us to investigate the impact of the proposed method to deterministic and ensemble nowcasts, respectively.

The key methodological components include: (1) CSGD modelling, (2) spatial structure analysis and interpolation, and (3) STEPS nowcasting and adjustment, which will be detailed in the following sections.

https://doi.org/10.5194/egusphere-2025-4590
Preprint. Discussion started: 6 January 2026

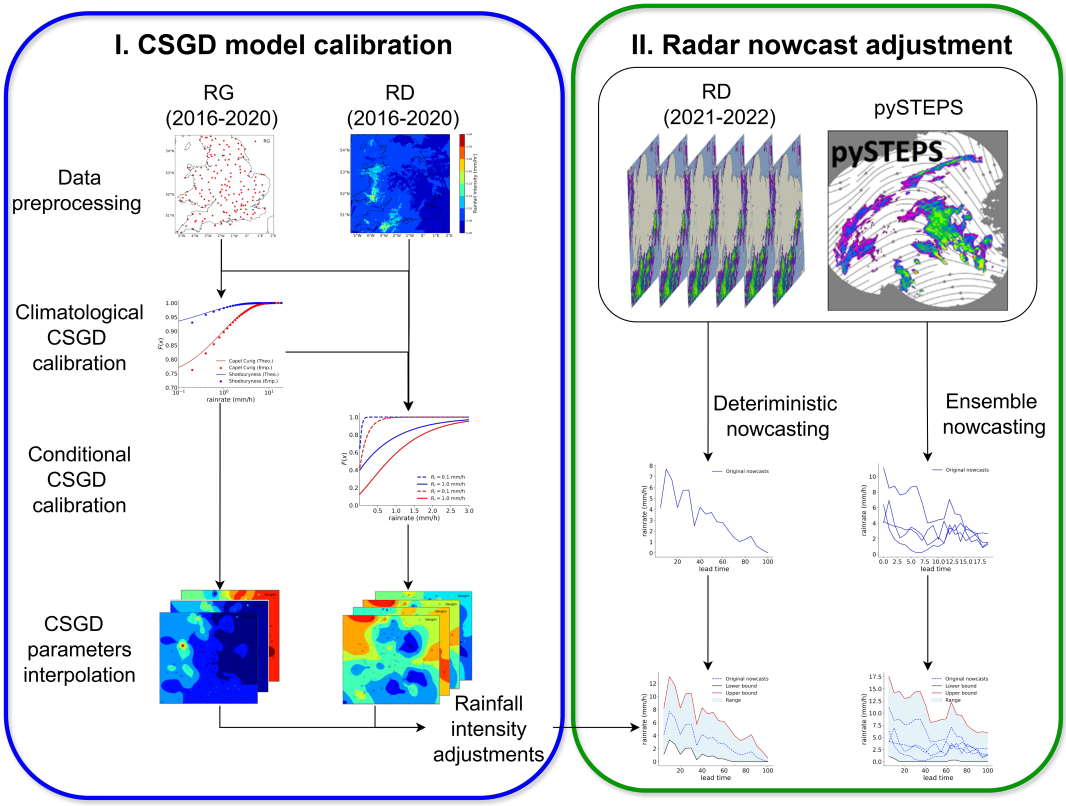

Figure 3. The proposed method to enhance the applicability of radar rainfall nowcasts to hydrological uses.

3.2 Censored Shifted Gamma Distribution (CSGD) Modelling

Early studies have demonstrated that the two-parameter gamma distribution is well-suited for modeling wet-day precipitation, supported by traditional goodness-of-fit tests (Ye et al., 2018; Hanson and Vogel, 2008). This distribution is widely used due to its simplicity, requiring only two parameters –derived from the mean and standard deviation of wet-day rainfall– to effectively represent precipitation probability (Chowdhury et al., 2017). However, precipitation modelling is inherently complex, as it involves both discrete and continuous processes: the occurrence of rainfall is discrete, whereas rainfall amounts are continuous. To capture both aspects within a unified framework, Scheuerer and Hamill (2015) introduced the Censored Shifted Gamma Distribution (CSGD) model.

A typical CSGD model comprises two components: the climatological and the conditional. The climatological component characterises the general distribution of precipitation, capturing spatial variations in precipitation magnitude and the probability of precipitation (POP). This component is typically constructed using high-quality reference data, such as rain gauge observations, to reflect long-term climatology. In contrast, the conditional CSGD model addresses systematic biases in remotely-sensed precipitation data (e.g., radar-derived rainfall rates) by modelling the relationship between radar estimates and true precipita-

https://doi.org/10.5194/egusphere-2025-4590
Preprint. Discussion started: 6 January 2026

tion. This model is essential for correcting errors –whether in a linear or nonlinear manner– and providing a conditional distribution that improves the accuracy of precipitation estimates.

While the CSGD framework has primarily been applied at daily timescales Baran and Nemoda (2016); Liu et al. (2019); Hartke et al. (2020), this study adapts it for hourly rainfall data. Specifically, we adopt the parameter estimation approach proposed by Scheuerer and Hamill (2015), which minimises the continuous ranked probability score (CRPS) between empirical and theoretical cumulative distribution functions (CDFs). Hourly GR data from 2016 to 2020 are used to calibrate the climatological CSGD model, while concurrent hourly RR and GR data are employed to calibrate the conditional CSGD models.

Further details on the calibration of the climatological and conditional CSGD models are provided in the following sections.

3.2.1 Climatological CSGD

In the climatological CSGD model, rainfall occurrence is conceptualised as a Bernoulli trial, governed by the POP. Once rainfall occurs, the rainfall amount is modelled using a gamma distribution with two parameters: the shape parameter k and the scale parameter θ. Both parameters can be reparameterised in terms of (climatological) mean (μ_c) and standard deviation (σ_c), as shown in Eq.1:

$$\mathrm{k} = \frac{\mu_c^2}{\sigma_c^2},\ \theta = \frac{\sigma_c^2}{\mu_c} \tag{1}$$

To address the limitation of the standard gamma distribution in representing the occurrence of climatological zero rainfall, a shift parameter δ is introduced, with $\delta < 0$. This parameter shifts the distribution leftward and censors all negative values at zero, thus enabling the model to capture the occurrence of dry periods. As a result, the cumulative distribution function (CDF) satisfies $F_{k,\theta,\delta}(0) = 1 - \mathrm{POP}$ and is defined as:

$$F_{k,\theta,\delta_c}(x) = \begin{cases} F_{k,\theta}(x - \delta_c) & \text{for } x \geq 0 \\ 0 & \text{for } x < 0 \end{cases} \tag{2}$$

3.2.2 Conditional CSGD

Building upon the parameters of the calibrated climatological CSGD model (i.e., μ_c, σ_c, and δ_c), the conditional CSGD model further refines the CDFs of 'true' rainfall intensity by conditioning on radar observations, $R_r(t)$, at time t. In this study, two versions of the conditional CSGD models are adopted: one based on linear relationships and the other based on nonlinear relationships (Wright et al., 2017).

Both versions share identical formulations for $\sigma(t)$ and $\delta(t)$, as shown in Eq.3 and Eq.4, respectively:

$$\sigma(t) = \alpha_4 \sigma_c \sqrt{\frac{\mu(t)}{\mu_c}} \tag{3}$$

https://doi.org/10.5194/egusphere-2025-4590
Preprint. Discussion started: 6 January 2026

$$\delta(t) = \delta_c \tag{4}$$

The key difference lies in how $\mu(t)$ relates to $R_r(t)$. In the linear version, $\mu(t)$ is directly proportional to $R_r(t)$ (see Eq.5), whereas in the nonlinear version, a nonlinear transformation is applied (see Eq.6).

$$\mu(t) = \mu_c \left[\alpha_2 + \alpha_3 \frac{R_r(t)}{\overline{R_r}}\right] \tag{5}$$

$$\mu(t) = \frac{\mu_c}{\alpha_1} \log1p\left\{\mathrm{expm1}(\alpha_1)\left[\alpha_2 + \alpha_3 \frac{R_r(t)}{\overline{R_r}}\right]\right\} \tag{6}$$

In these equations, $\log1p(x)$ denotes $\log(1+x)$, and $\mathrm{expm1}(x)$ denotes $\exp(x)-1$. In addition, $\overline{R_r}$ represents the mean radar based rainfall observation $R_r(t)$ over the calibration period.

3.3 Spatial structure analysis and interpolation of CSGD parameters

The outcome of the CSGD modelling is a set of CSGD parameters at rain-gauge locations. To apply these parameters across the RR gridded locations, spatial interpolation is required. Two interpolation techniques are tested for each CSGD parameter, and the method yielding the smallest mean absolute errors (MAEs, see definition in Eq. 7) is adopted for further application. In Eq. 7, N denotes the number of validation gauges, while θ_{clb} and θ_{intr} represent the calibrated and interpolated CSGD parameters, respectively.

$$\mathrm{MAE} = \frac{1}{N}\sum_{n=1}^{N} |\theta_{clb} - \theta_{intr}| \tag{7}$$

The first technique is ordinary Kriging (OK), which starts with variogram fitting –a fundamental geostatistical technique used to analyse the spatial structure of data. In this study, variogram fitting evaluates multiple parameter sets across various theoretical variogram models to identify the best fit to the spatial variance structure of each CSGD parameter. Typically, the empirical (or sample) variogram is first calculated from the data to estimate spatial variance as a function of distance. Several pre-selected theoretical variogram models –such as linear, spherical, exponential, and Gaussian– are then tested to determine which model best represents the empirical variogram.

Mathematically, this involves minimising the weighted squared errors between the empirical variogram ($\hat{\gamma}(h_i)$) and the theoretical variogram ($\gamma(h_i;\theta)$), where h_i denotes the distance between data pairs, and θ represents the variogram model parameters (sill, range, and nugget), as expressed in Eq.8.

$$(\hat{\theta}, \hat{M}) = \underset{\theta, M}{\arg\min} \sum_{i=1}^{N} w_i \left(\hat{\gamma}(h_i) - \gamma_M(h_i;\theta)\right)^2 \tag{8}$$

https://doi.org/10.5194/egusphere-2025-4590
Preprint. Discussion started: 6 January 2026

where γ_M represents a given theoretical variogram model. The weights, w_i, are proportional to the number of distance pairs in each bin, ensuring that distance classes with greater data density have a larger influence on the fitting process.

Optimisation is undertaken using the Trust Region Reflective (TRR) algorithm, known for its effectiveness in solving non-linear least squares problems in variogram fitting (Levenberg, 1944). Here, the nugget effect is assumed to be zero, reflecting minimal short-range variability. This assumption is justified by the use of quality-controlled GR/RR data for calibrating CSGD parameters, which minimises the influence of measurement errors. Furthermore, given the spatial resolution and scale of the study area, it is unnecessary to model ultra short-range variations typically represented by the nugget effect.

Based on the results of the spatial structure analyses, OK is applied to interpolate the CSGD parameter sets across radar gridded locations. OK operates under the assumption that the parameter of interest exhibits spatial correlation, as captured by a variogram, and that the mean of the parameter is constant but unknown throughout the study region. The interpolation is performed by assigning weights to neighbouring data points, with these weights determined by both the variogram model and the distances between known and unknown points (see Eq.9).

Mathematically, the estimate at an unknown location, $Z^*(x_0)$, is expressed as a weighted sum of the observed values at neighbouring locations, $Z(x_i)$:

$$Z^*(x_0) = \sum_{i=1}^{n} \lambda_i Z(x_i) \tag{9}$$

where λ_i are the Kriging weights, and n is the number of known locations used in the interpolation. These weights are obtained by solving the so-called Kriging system –a set of linear equations derived from the variogram model. This system ensures that the interpolation is unbiased and that the estimation error variance is minimised (Supajaidee et al., 2024; Huang et al., 2017; Wang and Li, 2017). OK thus effectively incorporates both the spatial correlation and the distribution of available data points, making it a robust technique for spatial prediction.

The alternative interpolation technique employed in this study is radial basis function (RBF) interpolation. Likewise, RBF interpolation is robust for estimating values at unknown locations based on known values. The core idea behind RBF is to construct a smooth, continuous surface that passes through all known data points, ensuring gradual and realistic spatial transitions. In this context, a smooth surface refers to one that minimises abrupt changes or irregularities, thus effectively capturing the spatial variability of parameters across the study area. The influence of each known location decreases with distance, governed by a radial basis function, ϕ. Common choices for ϕ include Gaussian, multiquadric, inverse multiquadric and thin-plate spline functions (Buhmann, 2000). Mathematically, RBF interpolation is formulated as:

$$f(\mathbf{x}) = \sum_{i=1}^{N} \lambda_i \phi(\|\mathbf{x} - \mathbf{x}_i\|) \tag{10}$$

where $f(\mathbf{x})$ is the interpolated value at an unknown location $\mathbf{x}$, N is the number of known locations, λ_i are the weights, $\mathbf{x}_i$ are the known locations, and $\phi(\|\mathbf{x} - \mathbf{x}_i\|)$ is the radial basis function evaluated based on the distance between $\mathbf{x}$ and $\mathbf{x}_i$.

https://doi.org/10.5194/egusphere-2025-4590
Preprint. Discussion started: 6 January 2026

The weights λ_i are determined by solving a system of linear equations based on the known data points. Specifically, for a set of N known locations with values $f(\mathbf{x}_i)$, the system of equations can be written as:

$$\begin{bmatrix} \phi(\|\mathbf{x}_1 - \mathbf{x}_1\|) & \phi(\|\mathbf{x}_1 - \mathbf{x}_2\|) & \cdots & \phi(\|\mathbf{x}_1 - \mathbf{x}_N\|) \\ \phi(\|\mathbf{x}_2 - \mathbf{x}_1\|) & \phi(\|\mathbf{x}_2 - \mathbf{x}_2\|) & \cdots & \phi(\|\mathbf{x}_2 - \mathbf{x}_N\|) \\ \vdots & \vdots & \ddots & \vdots \\ \phi(\|\mathbf{x}_N - \mathbf{x}_1\|) & \phi(\|\mathbf{x}_N - \mathbf{x}_2\|) & \cdots & \phi(\|\mathbf{x}_N - \mathbf{x}_N\|) \end{bmatrix} \begin{bmatrix} \lambda_1 \\ \lambda_2 \\ \vdots \\ \lambda_N \end{bmatrix} = \begin{bmatrix} f(\mathbf{x}_1) \\ f(\mathbf{x}_2) \\ \vdots \\ f(\mathbf{x}_N) \end{bmatrix}$$

In this system, the left-hand matrix represents the pairwise distances between all known locations, evaluated using the radial basis function ϕ, while the right-hand vector contains the observed values. Solving this system yields the weights, $\boldsymbol{\lambda} = [\lambda_1, \lambda_2, \ldots, \lambda_N]^T$, which remain constant throughout the interpolation process.

This technique ensures that the interpolated surface exactly passes through all known data points, providing a smooth and continuous spatial representation. Furthermore, the flexibility in selecting different radial basis functions allows RBF interpolation to adapt to a variety of spatial patterns and scales, making it a useful tool for interpolating CSGD parameters.

3.4 STEPS nowcasting and adjustment

3.4.1 STEPS: deterministic and ensemble nowcasting

STEPS is a stochastic nowcasting framework widely used for producing high-resolution ensemble precipitation forecasts (Bowler et al., 2006). Due to its capability to capture the spatial and temporal evolution of precipitation systems effectively, STEPS is widely recognised as one of the state-of-the-art nowcasting methods that has been used as a benchmark in many precipitation nowcasting developments (Ravuri et al., 2021; Shakti et al., 2015; Lugt et al., 2021). It builds upon a deterministic core that extrapolates radar-derived precipitation fields forward in time based on a motion field estimated from optical flow algorithms (e.g. Lucas–Kanade). This advection step assumes that the spatial structure of precipitation remains constant while being transported by the pre-determined flow, yielding a deterministic forecast of future rainfall distribution.

To capture the inherent uncertainty in short-term precipitation forecasting, particularly for convective rainfall, STEPS extends this deterministic approach into an ensemble one through introducing scale-dependent stochastic perturbations. This is achieved by decomposing the precipitation field using the Spectral Prognosis (S-PROG) method, which separates a given field into multiple fields representing respective spatial–scale features (Seed, 2003). While large-scale components, being more predictable, are preserved, small-scale features –characterised by higher variability– are perturbed with random noise sampled from fitted statistical distributions.

In this study, we conducted the STEPS nowcasting using the open-source pySTEPS library (Pulkkinen et al., 2019) and rely solely on radar observations as input. The deterministic component is first computed by estimating the motion field from a sequence of radar images, followed by the advection of the current precipitation field. The ensemble extension is then generated by applying stochastic perturbations to the small-scale components of the field at each time step.

https://doi.org/10.5194/egusphere-2025-4590
Preprint. Discussion started: 6 January 2026

The perturbations are designed to grow with lead time, reflecting the decay of predictability at finer spatial scales. By generating multiple realisations with different stochastic seeds, pySTEPS produces a set of ensemble members that evolve independently but are statistically consistent with the observed precipitation field.

For this study, we generate a total of 100 ensemble members, each representing a plausible evolution of future rainfall fields under the same large-scale motion but with different small-scale perturbations.

3.4.2 Adjustment of STEPS nowcasts

For both deterministic and ensemble nowcasting, the predicted rain rates at each gridded location (initially in mm/h) are first transformed into a cumulative distribution function (CDF) using the corresponding conditional CSGD models –both linear and non-linear variants. This transformation allows the derivation of a probabilistic rainfall distribution at each location. From each conditional CSGD, the median estimate is selected as the adjusted rainfall intensity for subsequent comparison with GR measurements and computation of error metrics.

Although the conditional CSGD mean is always nonzero and often exceeds the median —particularly in low-rainfall cases where the median may reasonably approach zero –it is generally less suitable as a central tendency measure. As discussed by Wright et al. (2017), the median offers several advantages over the mean:

1. Robustness to outliers: Precipitation data often include extreme values, and the median is less sensitive to such anomalies, making it a more stable and reliable indicator than the mean, which can be skewed by outliers.

2. Suitability for skewed distributions: The conditional CSGD typically produces right-skewed distributions, where the mean is biased by the extended upper tail. The median, by contrast, better represents the central value of asymmetrical precipitation distributions.

By addressing these considerations, the use of the median ensures a more robust and representative estimate of rainfall intensity for evaluating model performance.

3.5 Evaluation methodology

The evaluation of the proposed method involves two main parts. The first part assesses the accuracy of the CSGD model parameter estimation at ungauged (or unknown) locations. The second evaluates the quality of the adjusted nowcasts generated using the proposed CSGD method. Details are provided below of methods for evaluating each part.

3.5.1 Evaluating CSGD model parameters at unknown locations

To evaluate the effectiveness of interpolating the CSGD parameter sets, data from 10% of the rain-gauge stations (equivalent to 15 stations) from the MIDAS dataset were withheld from the list of known locations and used for validation. The selection of these validation stations was conducted by clustering all 156 stations into 15 groups using the K-means algorithm, with the station closest to the centre of each cluster excluded from the interpolation but still retained for model calibration. The

https://doi.org/10.5194/egusphere-2025-4590
Preprint. Discussion started: 6 January 2026

remaining 90% of rain-gauges (141 stations) were used to interpolate the CSGD parameter fields using both OK and radial basis function (RBF) approaches. For validation, the interpolated parameter values at the excluded stations are compared against their directly calibrated values, where absolute error is used as the performance metric. Eventually, the interpolation method yielding the lowest MAE for a given model parameter across all validation stations is selected as the preferred interpolation method.

3.5.2 Evaluating adjustment of nowcasted rainfall data

Unlike the model parameter evaluation, the radar nowcasts adjustment is based on MIDAS gauge records from all 156 stations for 2016–2020, with data from 2021–2022 reserved for validation. The EA-ST rainfall records, by contrast, are used only for validation, specifically to assess adjustment performance at the 5 min timescale.

The evaluation framework for deterministic and ensemble nowcasts follows a similar structure. In both cases, adjusted outputs –derived using linear and nonlinear conditional CSGD models– are compared against the original nowcasts, with GR observations serving as the reference. The key difference is that, for deterministic nowcasts, comparisons are undertaken directly against the GR observations, whereas for ensemble nowcasts, the comparisons involve the GR values and each ensemble member.

Temporal aggregation is dataset-specific: for MIDAS, 5 min nowcasts are aggregated to hourly intervals (up to a 6 h lead time) after adjustment; for EA-ST, adjustments are applied directly at the native 5 min resolution (up to a 3 h lead time).

To evaluate both deterministic and ensemble nowcasts across lead times, the Root Mean Squared Error (RMSE), the percentage reduction in RMSE following adjustment and the RMSE spreads are computed at given lead times. These are defined as:

- **Root Mean Square Error (RMSE)** quantifies the average magnitude of errors between nowcasted rainfall and gauge observations:

$$\mathrm{RMSE} = \sqrt{\frac{1}{N}\sum_{t=1}^{T}\sum_{l=1}^{L}(RN_{t,l} - GR_{t,l})^2} \tag{11}$$

  where $RN_{t,l}$ and $GR_{t,l}$ denote radar nowcasts and observed gauge records at time t and location l, respectively. T and L are the number of timestamps and locations, and $N = T \times L$ is the total number of comparison pairs.

- **Reduction (%) in RMSEs** is used to measure the relative improvement in performance after CSGD based adjustment:

$$\Delta\mathrm{RMSE}\ (\%) = \frac{\mathrm{RMSE}_{\mathrm{org}} - \mathrm{RMSE}_{\mathrm{adj}}}{\mathrm{RMSE}_{\mathrm{org}}} \times 100 \tag{12}$$

  where $\mathrm{RMSE}_{\mathrm{org}}$ and $\mathrm{RMSE}_{\mathrm{adj}}$ represent the RMSE calculated using the original and the adjusted nowcasts, respectively.

- **Dispersion of RMSEs** is used to quantify the variability of nowcasting errors:

$$\mathrm{RMSE}_{I_{90}} = \mathrm{RMSE}_{q_{95}} - \mathrm{RMSE}_{q_5} \tag{13}$$

  where RMSE_{q_5} and $\mathrm{RMSE}_{q_{95}}$ denote the 5th and 95th percentiles of the RMSE distributions of nowcasts.

https://doi.org/10.5194/egusphere-2025-4590
Preprint. Discussion started: 6 January 2026

In addition, two complementary metrics are employed to capture specific aspects of performance:

– **Pearson Correlation Coefficient** (ρ_{Pearson}) quantifies the linear similarity between observed and nowcasted rainfall at a given lead time:

$$\rho_{\text{Pearson}} = \frac{\sum_{t=1}^{T}\sum_{l=1}^{L}(GR_{t,l} - \overline{GR})(RN_{t,l} - \overline{RN})}{\sqrt{\sum_{t=1}^{T}\sum_{l=1}^{L}(GR_{t,l} - \overline{GR})^2}\sqrt{\sum_{t=1}^{T}\sum_{l=1}^{L}(RN_{t,l} - \overline{RN})^2}} \tag{14}$$

where $\overline{GR}$ and $\overline{RN}$ represent the mean values of gauge observations and nowcasts, respectively.

– **Overall Bias (OB)** measures systematic deviation from the observations:

$$\text{OB} = \frac{\sum_{t=1}^{T}\sum_{l=1}^{L} RN_{t,l}}{\sum_{t=1}^{T}\sum_{l=1}^{L} GR_{t,l}} \tag{15}$$

To further investigate the influence of the CSGD based adjustment on nowcasting uncertainties, a variance decomposition is performed. Specifically, at each lead time, the variance of the difference between the original and adjusted nowcasts is expressed in terms of their deviations from GR and the covariance between these deviations:

$$\text{Var}[RN_{orig.} - RN_{adj.}] = \text{Var}[RN_{orig.} - GR] + \text{Var}[RN_{adj.} - GR] - 2\text{Cov}[RN_{orig.} - GR, RN_{adj.} - GR] \tag{16}$$

Here, $\text{Var}[RN_{orig.} - GR]$ and $\text{Var}[RN_{adj.} - GR]$ denote the error variances of the original and adjusted nowcasts relative to GR, respectively, while $\text{Cov}[RN_{\text{orig}} - GR, , RN_{\text{adj}} - GR]$ represents the covariance between these two errors.

The key focus lies on the reduction from $\text{Var}[RN_{\text{orig}} - GR]$ to $\text{Var}[RN_{\text{adj}} - GR]$ across lead times. This provides insights into how algorithmic and measurement-related uncertainties evolve with lead time, and demonstrates the extent to which the CSGD models mitigate nowcasting uncertainty.

4 Results and discussion

4.1 Performance of CSGD parameter calibration and interpolation

The calibration of the CSGD parameters reveals clear spatial associations across the study domain (Figure 4), supporting the feasibility of spatial interpolation over the radar grids. Higher values of the climatological mean (μ) and standard deviation (σ) are particularly evident in orographically influenced areas, consistent with known regional precipitation gradients and confirming the reliability of the calibration.

A notable example is the gauge station 'CAPEL CURIG NO 3' ($3.941°$W, $53.094°$N) in North Wales, which, according to Met Office (a), records an average annual rainfall of 2697.13 mm –one of the highest in the UK– due to strong orographic lifting over mountainous terrain. During extreme events, such as those in February 2004, this station recorded 297 mm of rainfall over three days, with hourly intensities reaching 6–7 mm (Sibley, 2005). This explains the exceptionally high μ and σ values observed at this site.

https://doi.org/10.5194/egusphere-2025-4590
Preprint. Discussion started: 6 January 2026

To enable pixel-wise application of the CSGD models, spatial interpolation was performed using both OK and Radial Basis Function (RBF) methods. As described in Section 3.5.1, a cross-validation strategy was adopted, withholding 10% of the MIDAS stations from interpolation to evaluate accuracy using MAE.

A spatial structure analysis was first conducted for each CSGD parameter. The sample variogram for each model parameter was fitted using selected theoretical models (i.e. stable, exponential and Gaussian), confirming moderate spatial autocorrelation with most sills reached within 500 km (Figure 5). The best-fitting variogram models, selected based on the highest R^2 and lowest weighted least squares (WLS), were used for OK interpolation (detailed results provided in the Supplement).

For comparison, RBF interpolation was conducted using various basis functions (i.e., cubic, Gaussian, multiquadric and thin-plate spline). As shown in Figure 6, although the optimal method varied by parameter, RBF generally outperformed OK in terms of MAE. The combination of the variogram model or basis function yielding the lowest MAE was eventually selected to generate the final gridded CSGD parameter fields (Figure 7). These fields serve as the foundation for pixel-wise CSGD adjustments of both deterministic and ensemble radar based nowcasts.

https://doi.org/10.5194/egusphere-2025-4590
Preprint. Discussion started: 6 January 2026

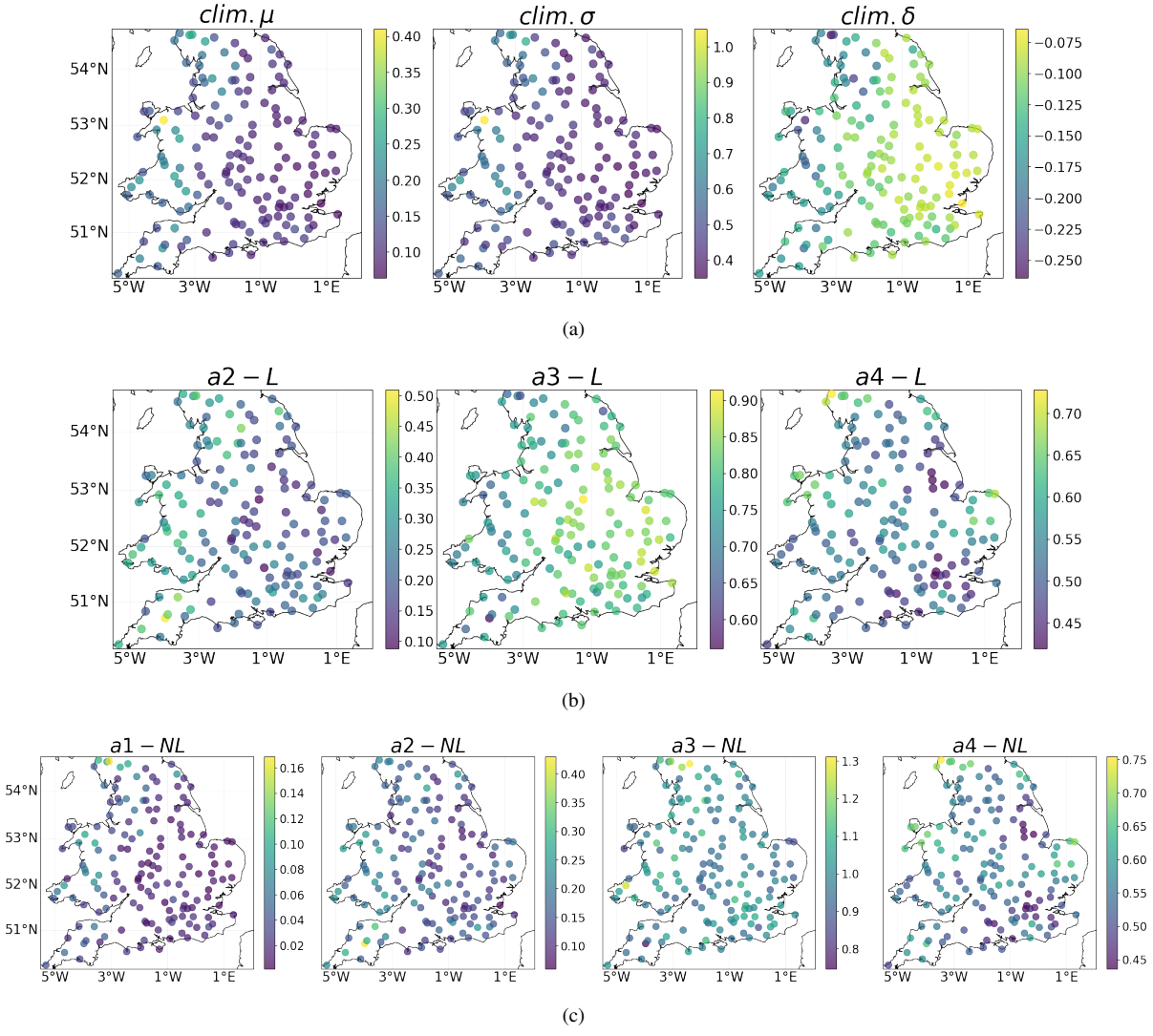

Figure 4. Calibrated CSGD parameter sets on gauge locations (MIDAS). (**a**) Climatological CSGD; (**b**) Conditional CSGD (Linear); (**c**) Conditional CSGD (Non-Linear).

https://doi.org/10.5194/egusphere-2025-4590
Preprint. Discussion started: 6 January 2026

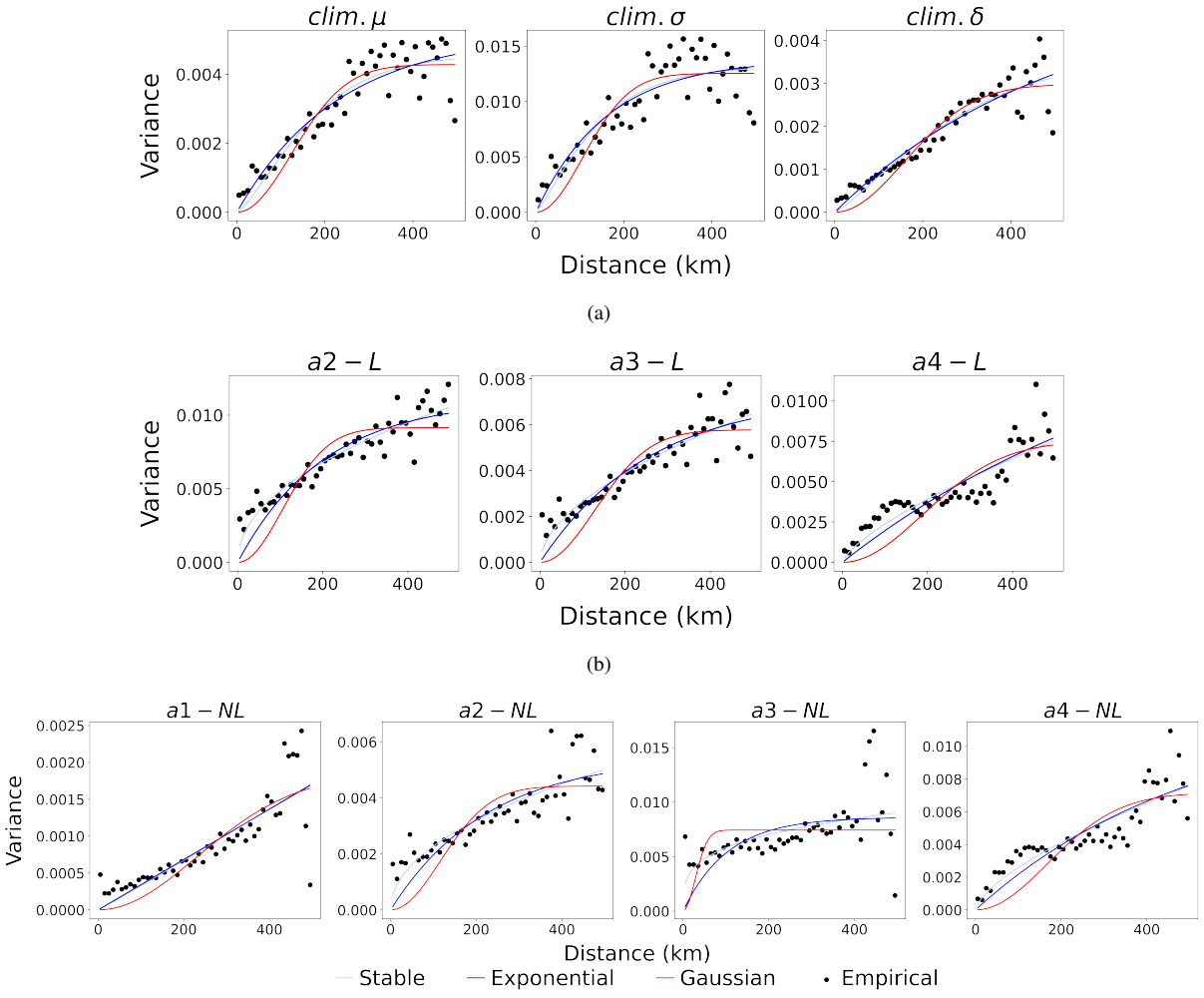

Figure 5. Variogram fitting of CSGD parameter sets by common variogram models. (**a**) Climatological CSGD; (**b**) Conditional CSGD (Linear); (**c**) Conditional CSGD (Non-Linear).

https://doi.org/10.5194/egusphere-2025-4590
Preprint. Discussion started: 6 January 2026

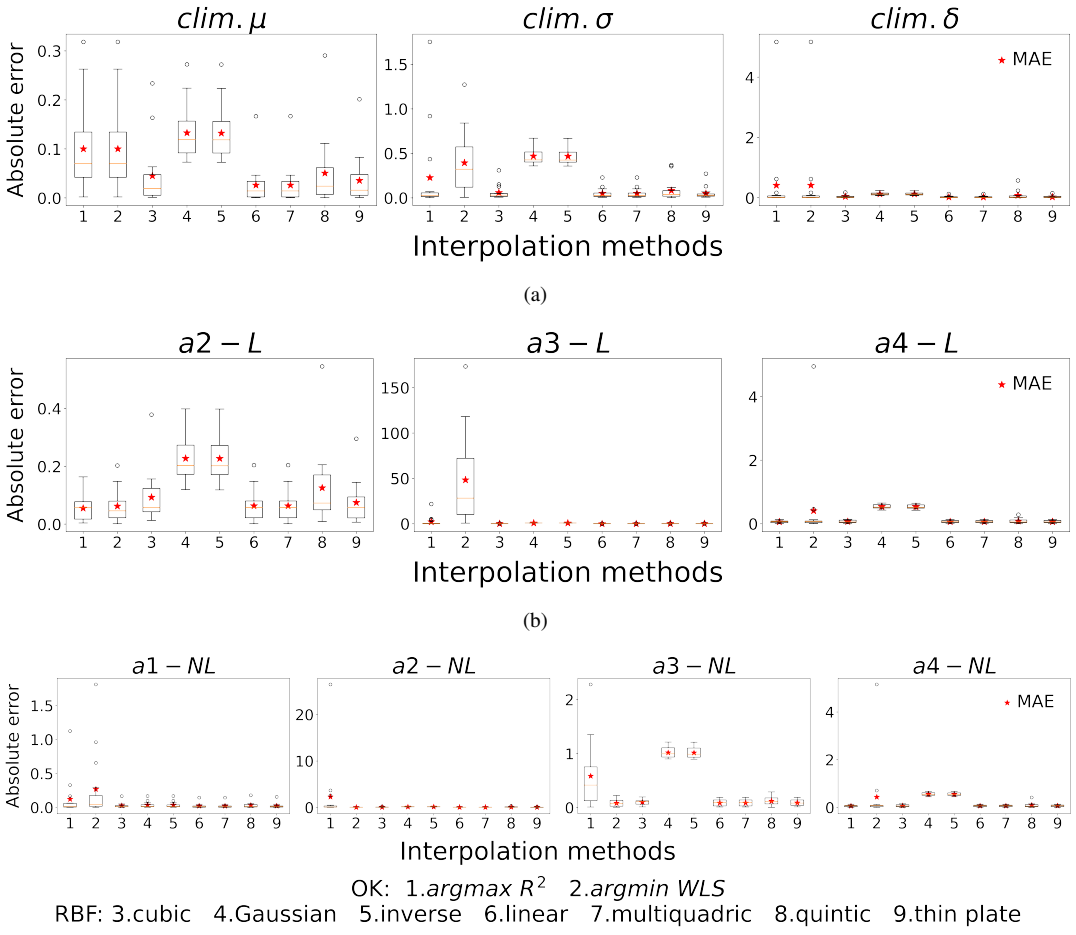

Figure 6. Evaluations of spatial interpolation methods on CSGD parameter sets by MAE. (**a**) Climatological CSGD; (**b**) Conditional CSGD (Linear); (**c**) Conditional CSGD (Non-Linear). Methods 1 and 2 are OK based interpolations resulting from the 'best' variogram models obtained from the highest R^2 and the lowest weighted least square (WLS) errors. Methods 3–9 are RBF based interpolations using various radial basis functions.

https://doi.org/10.5194/egusphere-2025-4590
Preprint. Discussion started: 6 January 2026

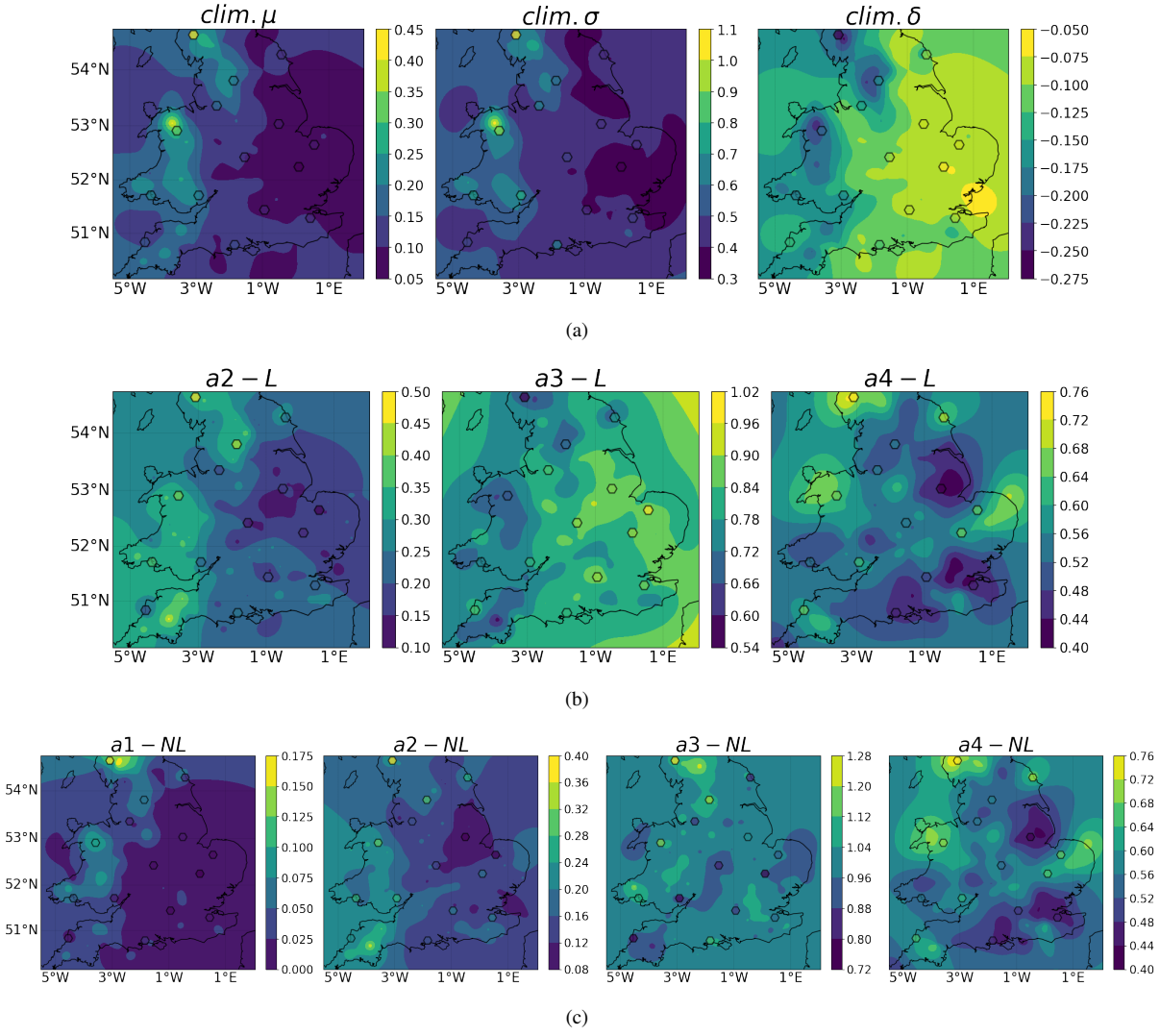

(a)

(b)

(c)

Figure 7. Optimal interpolated fields of CSGD parameter sets. (**a**) Climatological CSGD; (**b**) Conditional CSGD (Linear); (**c**) Conditional CSGD (Non-Linear).

4.2 Performance of CSGD based nowcast adjustment

4.2.1 Predictive performance

We first observe the overall performance across 6 (MIDAS data) and 3 h (EA-ST data) forecast lead times for all selected events. We then categorises events into *summer* and *winter* events. As listed in Table 1, *summer* events are defined as those occurring between 15 April and 15 October, yielding a total of 11 events, whereas the remaining 9 cases are classified as *winter* events. Note that for readability, we only present results assessed from comparing with MIDAS 1 h gauge data. The results with EA-ST 5 min gauge records are provided in the Appendices.

https://doi.org/10.5194/egusphere-2025-4590
Preprint. Discussion started: 6 January 2026

The evaluation begins with the RMSE evaluations for deterministic and ensemble nowcasting on the MIDAS dataset are presented in Figure 8 and Figure 9, and the RMSE dispersions are listed in Table 2. We can observe that:

- The CSGD adjustment generally results in more pronounced improvements in winter than in summer, regardless of the nowcasting scenario or temporal resolution.
- For deterministic nowcasting, the degree of RMSE reduction increases progressively with lead time. For the MIDAS dataset, the reduction ranges from -2% at the first hour to 9% at the sixth hour. For the EA-ST dataset, the reduction rises from near 0% to 6% within the first 50 minutes and remains similar thereafter.
- The non-linear CSGD model consistently outperforms its linear counterpart across all lead times, datasets and nowcasting scenarios. the degree of RMSE reductions remain similar at approximately 6% across all lead times. This stability can be attributed to the incorporation of rainfall evolution stochasticity in ensemble nowcasting. The consistent improvement achieved by the non-linear CSGD model demonstrates its ability to effectively mitigate systematic measurement errors in nowcasts at both hourly and 5 min temporal resolutions.

The analysis of RMSE dispersions provides further insights into nowcasting uncertainty. As shown in Table 2 (and Tables A1 and A2), dispersions increase steadily with lead time for both deterministic and ensemble nowcasts, reflecting the progressive accumulation of uncertainty. In addition, the dispersions of RMSE appear largely insensitive to storm types –no significant differences in $\mathrm{RMSE}I90$ or their evolution across lead times are observed between summer and winter events. Importantly, across nearly all lead times, models and storm types, the non-linear CSGD adjustment consistently reduces RMSE dispersions. The magnitude of reduction becomes more pronounced at longer lead times for both the 1 h and 5 min temporal resolutions. These findings highlight the robustness of the non-linear CSGD model in reducing variability in nowcasting uncertainty under both deterministic and ensemble settings.

To further assess the predictive quality, we then examine correlation with GR observations (Table 3 for the MIDAS dataset, and Tables A3–A4 for EA-ST). Similar to the RMSE dispersion results, storm-type dependence is insignificant. Generally, the non-linear CSGD adjustment demonstrates a stronger ability to improve correlation with GR compared to the linear model. However, the impact of non-linear CSGD adjustments differs between datasets. At the 1 h scale (MIDAS), correlations consistently improve across all events and for both deterministic and ensemble nowcasts after adjustment. By contrast, at the 5 min scale (EA-ST), deterministic nowcasts show correlations that do not decrease monotonically with lead time, leading to non-uniform responses to adjustment and occasional deterioration.

We finally look into the unconditional bias aspect via overall bias (OB) evaluation (Table 4 for the MIDAS dataset, and Tables A5 and A6 for the EA-ST). The original deterministic and ensemble nowcasts are generally close to unbiased during the first 3 h lead time but progressively shift toward overestimation thereafter. In contrast, the CSGD-adjusted nowcasts tend to underestimate rainfall during the initial 3 h period yet effectively correct the subsequent overestimation. This early underestimation could be primarily attributable to the use of medians to represent adjusted nowcasts (see Sect. 3.4.2).

https://doi.org/10.5194/egusphere-2025-4590
Preprint. Discussion started: 6 January 2026

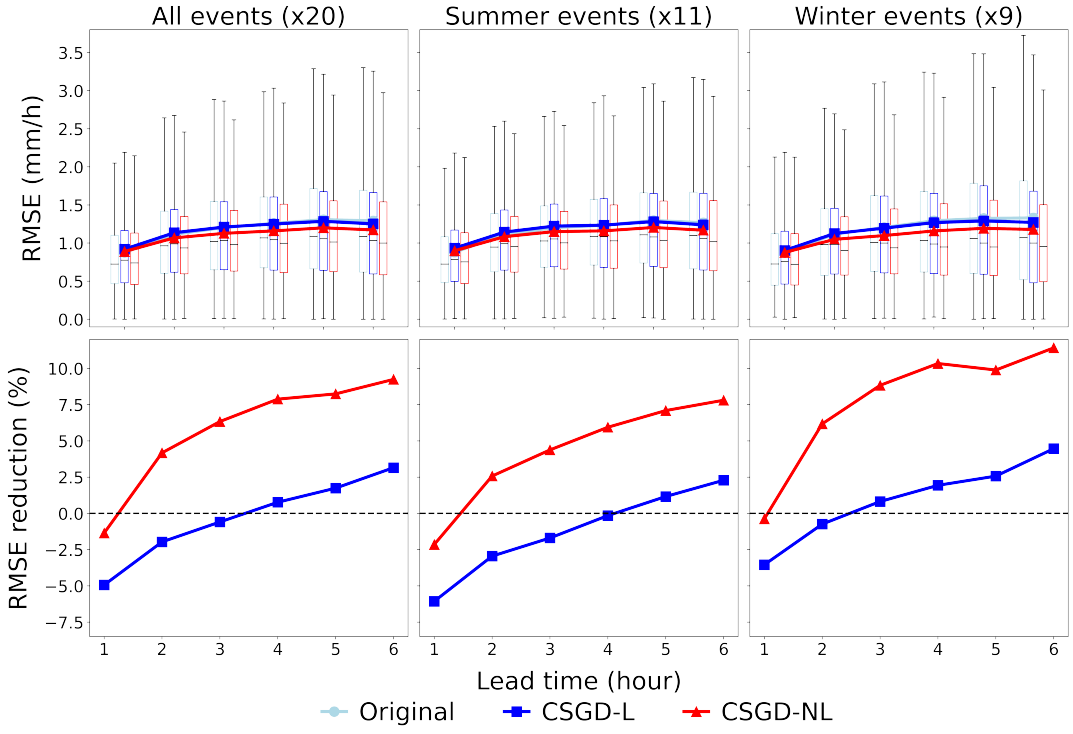

Figure 8. Variations in deterministic nowcasting errors (in terms of RMSEs, top row) and their reduction (in %, bottom row) across 1 to 6 h forecast lead times after applying CSGD based adjustments (MIDAS).

https://doi.org/10.5194/egusphere-2025-4590
Preprint. Discussion started: 6 January 2026

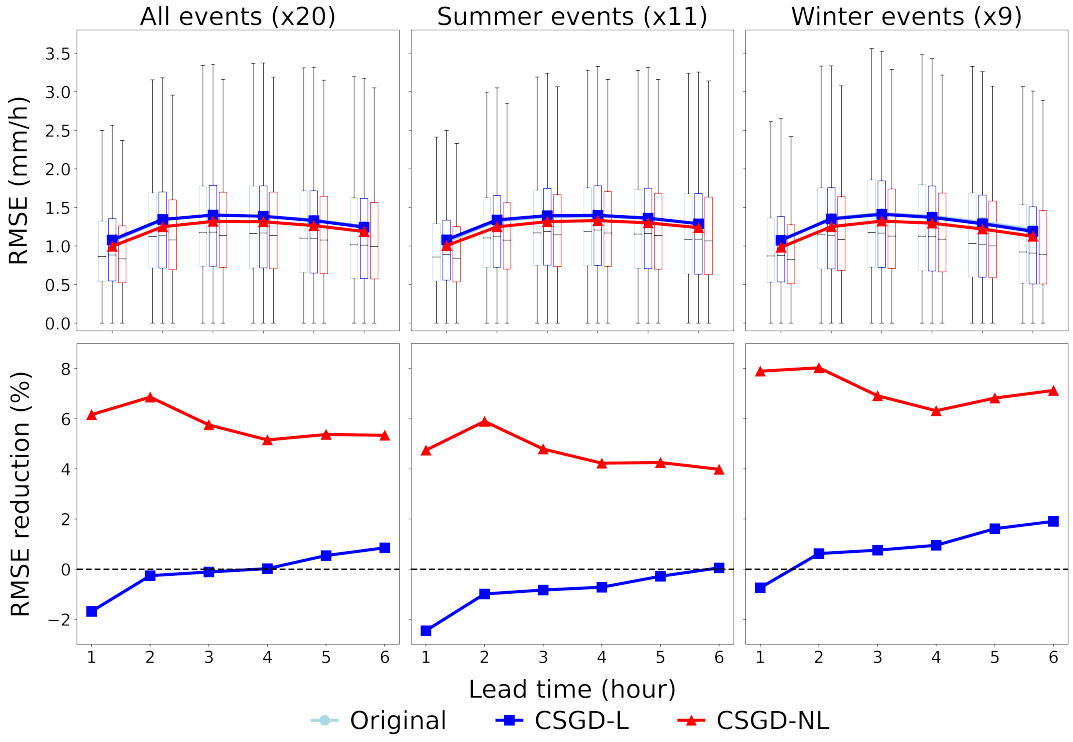

Figure 9. Variations in ensemble nowcasting errors (in terms of RMSEs, top row) and their reduction (in %, bottom row) across 1 to 6 h forecast lead times after applying CSGD based adjustments (MIDAS).

https://doi.org/10.5194/egusphere-2025-4590
Preprint. Discussion started: 6 January 2026

Table 2. Deterministic and ensemble nowcasting uncertainty (in terms of RMSE dispersions, $\mathrm{RMSE}_{I_{90}}$) across 1 to 6 h forecast lead times before and after applying CSGD-adjustments (MIDAS).

Lead time (hour)	All			Summer			Winter		
	Original	CSGD-L	CSGD-NL	Original	CSGD-L	CSGD-NL	Original	CSGD-L	CSGD-NL
	Deterministic								
1	**1.82**	1.94	1.85	**1.79**	1.97	1.88	1.85	1.92	**1.83**
2	2.24	2.24	**2.08**	2.21	2.27	**2.12**	2.27	2.25	**2.08**
3	2.42	2.45	**2.20**	2.35	2.36	**2.19**	2.51	2.51	**2.22**
4	2.67	2.66	**2.38**	2.47	2.52	**2.18**	2.91	2.88	**2.62**
5	2.86	2.82	**2.55**	2.52	2.58	**2.42**	3.12	3.18	**2.84**
6	2.96	2.90	**2.47**	2.62	2.59	**2.27**	3.23	3.16	**2.78**
	Ensemble								
1	2.25	2.27	**2.00**	2.22	2.25	**2.04**	2.29	2.29	**1.96**
2	2.75	2.72	**2.42**	2.70	2.69	**2.42**	2.80	2.76	**2.42**
3	2.87	2.84	**2.58**	2.80	2.77	**2.53**	2.96	2.94	**2.63**
4	2.92	2.90	**2.66**	2.83	2.83	**2.62**	3.04	2.99	**2.70**
5	2.99	2.95	**2.71**	2.90	2.89	**2.68**	3.08	3.03	**2.74**
6	2.85	2.80	**2.58**	2.80	2.79	**2.60**	2.92	2.84	**2.56**

Table 3. Pearson correlation coefficients between GR and original/CSGD-adjusted deterministic and ensemble nowcasts across 1 to 6 h forecast lead times (MIDAS).

Lead time (hour)	All			Summer			Winter		
	Original	CSGD-L	CSGD-NL	Original	CSGD-L	CSGD-NL	Original	CSGD-L	CSGD-NL
	Deterministic								
1	0.739	0.723	**0.747**	0.741	0.725	**0.753**	0.737	0.722	**0.741**
2	0.575	0.556	**0.581**	0.586	0.563	**0.588**	0.563	0.549	**0.572**
3	0.427	0.406	**0.442**	0.434	0.408	**0.445**	0.420	0.404	**0.438**
4	0.320	0.302	**0.332**	0.318	0.295	**0.332**	0.323	0.312	**0.332**
5	0.220	0.204	**0.228**	0.222	0.203	**0.231**	0.215	0.204	**0.223**
6	0.149	0.139	**0.156**	0.147	0.134	**0.155**	0.152	0.149	**0.159**
	Ensemble								
1	0.636	0.616	**0.666**	0.639	0.620	**0.668**	0.634	0.615	**0.663**
2	0.395	0.377	**0.422**	0.415	0.395	**0.446**	0.369	0.356	**0.391**
3	0.245	0.233	**0.267**	0.282	0.267	**0.310**	0.196	0.189	**0.209**
4	0.157	0.148	**0.173**	0.189	0.178	**0.212**	0.115	0.109	**0.121**
5	0.103	0.097	**0.114**	0.122	0.114	**0.138**	0.077	0.074	**0.080**
6	0.064	0.060	**0.071**	0.075	0.069	**0.085**	0.050	0.047	**0.051**

https://doi.org/10.5194/egusphere-2025-4590
Preprint. Discussion started: 6 January 2026

Table 4. Overall bias (OB) values between GR and original/CSGD-adjusted deterministic and ensemble nowcasts across 1 to 6 h forecast lead times (MIDAS).

Lead time (hour)	All			Summer			Winter		
	Original	CSGD-L	CSGD-NL	Original	CSGD-L	CSGD-NL	Original	CSGD-L	CSGD-NL
	Deterministic								
1	**0.927**	0.724	0.692	**0.880**	0.679	0.662	**0.997**	0.790	0.738
2	**0.963**	0.756	0.717	**0.899**	0.698	0.674	**1.060**	0.843	0.783
3	**1.031**	0.806	0.767	**0.956**	0.743	0.716	1.148	**0.906**	0.848
4	1.182	**0.919**	0.879	**1.085**	0.840	0.813	1.340	1.049	**0.987**
5	1.428	1.109	**1.060**	1.281	**0.988**	0.956	1.683	1.319	**1.237**
6	1.763	1.367	**1.308**	1.542	1.190	**1.148**	2.169	1.694	**1.599**
	Ensemble								
1	**0.965**	0.777	0.738	**0.927**	0.739	0.714	**1.023**	0.834	0.775
2	**0.985**	0.793	0.757	**0.939**	0.750	0.726	**1.056**	0.859	0.804
3	**1.043**	0.838	0.801	**0.979**	0.780	0.755	1.145	**0.931**	0.875
4	1.140	**0.914**	0.875	**1.049**	0.833	0.807	1.291	1.047	**0.986**
5	1.288	1.029	**0.987**	1.161	**0.918**	0.892	1.508	1.219	**1.152**
6	1.441	1.146	**1.105**	1.284	**1.011**	0.986	1.722	1.386	**1.317**

4.2.2 Variations in nowcast error variances

In addition to the predictive metrics described above, we further examine how nowcasting uncertainty evolves with lead time and how it is affected by the CSGD adjustment (see Figures 10 and 11 for the MIDAS dataset, and Figures B1 and B2 for the EA-ST dataset). The key findings include:

- The overall nowcasting uncertainty (expressed as the error variance between original nowcasts and ground gauge records $\mathrm{Var}[RN_{orig} - GR]$, dark solid lines) behaves differently in deterministic and ensemble settings. For deterministic nowcasts, uncertainty increases steadily with lead time. For ensemble nowcasts, uncertainty peaks around the 4 h lead time and then decreases slightly, suggesting that incorporating stochasticity helps capture rainfall evolution, thus effectively reducing nowcsting uncertainty. In the EA-ST dataset, where the forecast horizon is limited to 3 h, both deterministic and ensemble error variances increase monotonically with lead time.

- The non-linear CSGD model (green solid lines) consistently outperforms the linear CSGD model (orange solid lines) in reducing nowcasting uncertainty for both deterministic and ensemble cases. For deterministic nowcasts, uncertainty reduction becomes more evident as lead time increases, while for ensemble nowcasts the reduction remains relatively stable across lead times. On average, the non-linear CSGD adjustment achieves an uncertainty reduction of approximately 20% in the ensemble setting.

https://doi.org/10.5194/egusphere-2025-4590
Preprint. Discussion started: 6 January 2026

– The storm-type dependence of uncertainty reduction is negligible in the MIDAS dataset. In the EA-ST dataset, however, reductions are more pronounced in winter than in summer events. In particular, for deterministic nowcasts, CSGD adjustments provide the least impact on uncertainty reduction for summer events.

– In all cases, the non-linear CSGD model consistently produces higher error variances between the original and the adjusted nowcasts than the linear model across all lead times. This indicates that the non-linear model applies stronger adjustments than its linear counterpart.

Overall, these findings highlight the robustness of the non-linear CSGD model in reducing uncertainty across different datasets, lead times and storm types, thereby strengthening its suitability for operational hydrological applications.

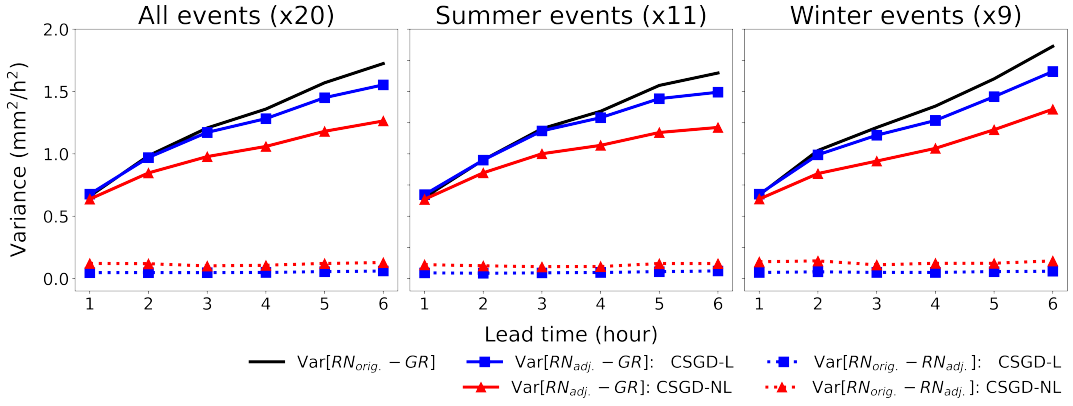

Figure 10. Error variances relative to gauge records for the original deterministic nowcasts and those adjusted using linear and non-linear CSGD models (MIDAS).

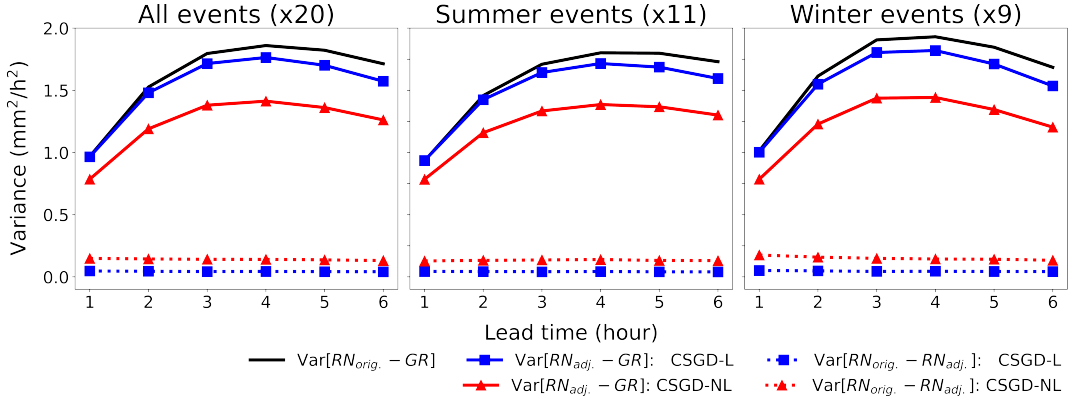

Figure 11. Error variances relative to gauge records for the original deterministic nowcasts and those adjusted using linear and non-linear CSGD models (MIDAS).

https://doi.org/10.5194/egusphere-2025-4590
Preprint. Discussion started: 6 January 2026

5 Conclusions

This study proposes a framework to enhance the applicability of radar based precipitation nowcasts in hydrological practice by integrating Censored Shifted Gamma Distribution (CSGD) models with nowcasts generated by the Short-Term Ensemble Prediction System (STEPS).

Originally developed to correct systematic biases and quantify uncertainty in satellite precipitation datasets at daily and ∼ 10 km scales, CSGD models are here adapted and extended to hourly (and sub-hourly) resolutions and ∼1 km spatial scales, within a nowcasting context. Both linear and non-linear conditional CSGD models are used to transform nowcasted rainfall intensities into conditional probability distributions, providing a flexible probabilistic representation that captures both the discrete and continuous nature of precipitation.

Our main contributions include:

- **Extending CSGD applicability via parameterisation and spatial interpolation.** We integrate CSGD parameter calibration with spatial interpolation techniques to extend the framework's applicability to regions without dense ground rainfall (GR) measurements. First, a spatial structure analysis confirms that the CSGD parameters exhibit spatial clustering. Then, multiple interpolation methods are tested to identify the optimal model for each parameter. This combined parameterisation–interpolation strategy effectively bridges observational gaps, enabling broader use of the CSGD framework in data-sparse regions—particularly relevant for operational hydrology.

- **Mitigating systematic biases and quantifying uncertainty in deterministic and ensemble nowcasting.** The framework addresses both error and uncertainty in nowcasting outputs. For deterministic nowcasts, where error and uncertainty typically increase with lead time, the non-linear CSGD model outperforms the linear model, offering greater bias correction and uncertainty reduction. For ensemble nowcasts, which inherently include stochastic perturbations to account for uncertainty, the non-linear CSGD model consistently achieves notable improvement –reducing prediction errors by nearly 6 % at 6 h (1 h scale) and 3 h (5 min scale) lead times, and narrowing uncertainty spreads across all lead times. These findings highlight the practical value of non-linear CSGD modelling for hydrological applications requiring robust and interpretable probabilistic nowcasts.

Despite these advancements, it is important to recognise the challenges that remain. The current strategy of selecting the median from the CSGD distribution as the adjusted rainfall intensity requires further examination. Under the assumption that precipitation follows a gamma distribution, this median based adjustment modifies the original rainfall intensity in only one direction. While this approach has shown effectiveness in reducing overall errors and uncertainties, it may inadvertently increase false alarms or missed detections when rainfall thresholds are applied. To overcome these limitations, future research could consider incorporating additional meteorological predictors and adopting machine learning methods. Unlike distribution based approaches, machine learning models are inherently non-linear and do not rely on predefined probability distributions, offering greater flexibility for refining rainfall adjustments and improving detection accuracy.

https://doi.org/10.5194/egusphere-2025-4590
Preprint. Discussion started: 6 January 2026

Code and data availability. The gauge datasets used in this study are available at https://doi.org/10.5281/zenodo.17181918 (Lin et al., 2025a), comprising 1-h rainfall data (2016–2022) from the Met Office MIDAS Open archive and 5-min rainfall records from the Environment Agency for the Severn Trent region (2021). The MIDAS data can be obtained through the Centre for Environmental Data Analysis (CEDA), while the EA-ST dataset can be requested directly from the Environment Agency (UK). Both two datasets have been re-formatted to CSV (Comma Separated Values) files. Nimrod radar data are also hosted by CEDA and are freely available for research use, subject to user registration. The Python scripts used to generate deterministic and ensemble nowcasts, calibrate and interpolate CSGD parameters, and perform verification and uncertainty decomposition has been archived at https://doi.org/10.5281/zenodo.17984774 (Lin et al., 2025b), which also includes the derived conditional CSGD parameter files (in HDF5 format) used in the analysis. The software tools used in this study are open source. The nowcasting framework pySTEPS is accessible at https://pysteps.readthedocs.io, and the CSGD error-modelling code is available at https://github.com/KaidiWisc/CSGD_error_model.

Appendix A: Predictive performance metrics: EA-ST

Figures A1 and A2 illustrate the RMSE reduction (in %) in deterministic and ensemble nowcasts across 1 to 3 h forecast lead times at 5 min timescales adjusted by linear and non-linear CSGD models. Note that the CSGD models here were calibrated using MIDAS data at the 1 h timescale, and were applied to 5 min EA-ST data. Tables A1-A6 summarise the corresponding uncertainty changes (in terms of $\mathrm{RMSE}_{I_{90}}$), pearson correlation coefficients and overall bias (OB) values against EA-ST gauge records.

https://doi.org/10.5194/egusphere-2025-4590
Preprint. Discussion started: 6 January 2026

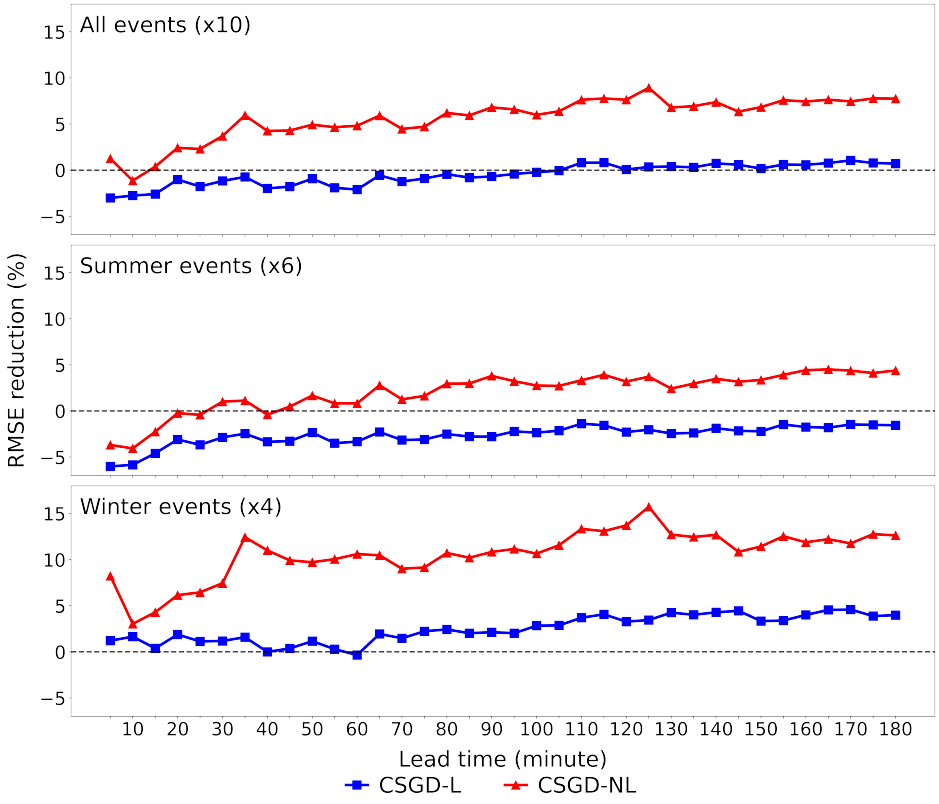

Figure A1. Variations in RMSE reduction (in %) of deterministic nowcasting across 1 to 3 h forecast lead times after applying CSGD based adjustments (EA-ST).

https://doi.org/10.5194/egusphere-2025-4590
Preprint. Discussion started: 6 January 2026

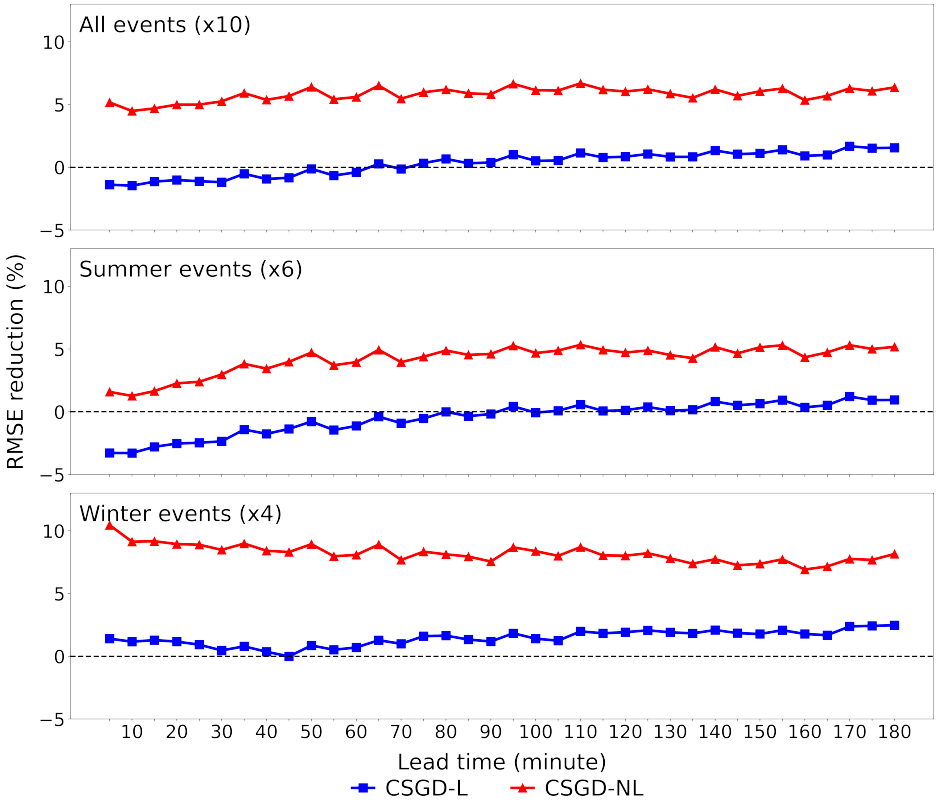

Figure A2. Variations in RMSE reduction (in %) of ensemble nowcasting across 1 to 3 h forecast lead times after applying CSGD based adjustments (EA-ST).

https://doi.org/10.5194/egusphere-2025-4590
Preprint. Discussion started: 6 January 2026

Table A1. Deterministic nowcasting uncertainty (in terms of RMSE dispersions, $\mathrm{RMSE}_{I_{90}}$) across 1 to 3 h forecast lead times before and after applying CSGD-adjustments (EA-ST).

Lead time (minute)	All			Summer			Winter		
	Original	CSGD-L	CSGD-NL	Original	CSGD-L	CSGD-NL	Original	CSGD-L	CSGD-NL
5	1.70	1.73	**1.62**	1.49	1.52	**1.43**	1.86	1.93	**1.74**
10	1.93	1.92	**1.79**	1.90	1.77	**1.77**	1.97	2.06	**1.70**
15	1.96	1.97	**1.95**	1.92	**1.87**	1.93	1.98	2.02	**1.60**
20	2.03	2.02	**1.91**	1.76	1.76	**1.69**	2.33	2.42	**2.29**
25	1.93	1.96	**1.78**	1.89	1.92	**1.78**	1.99	1.99	**1.80**
30	1.96	1.93	**1.76**	1.74	1.69	**1.64**	2.23	2.43	**2.19**
35	2.18	2.05	**1.81**	1.65	1.69	**1.62**	2.55	2.68	**2.11**
40	2.12	2.17	**1.97**	1.99	1.98	**1.96**	2.49	2.55	**1.95**
45	1.94	2.02	**1.87**	**1.82**	1.92	1.87	2.17	2.19	**1.88**
50	2.08	2.06	**1.90**	1.90	1.95	**1.86**	2.39	2.44	**1.95**
55	1.97	2.00	**1.76**	1.81	1.88	**1.78**	2.30	2.53	**1.65**
60	1.99	2.06	**1.72**	1.87	1.90	**1.71**	2.02	2.29	**1.74**
65	2.20	2.17	**1.83**	1.93	1.99	**1.79**	2.39	2.32	**1.87**
70	2.31	2.30	**2.10**	2.22	2.20	**2.09**	2.38	2.55	**2.07**
75	2.32	2.47	**2.12**	2.29	2.30	**2.10**	2.47	2.66	**2.01**
80	2.29	2.40	**2.05**	2.03	2.16	**1.97**	2.52	2.59	**2.33**
85	2.23	2.31	**1.96**	2.11	2.18	**1.84**	2.54	2.58	**2.04**
90	2.15	2.17	**2.00**	1.93	2.02	**1.75**	2.75	2.84	**2.23**
95	2.27	2.36	**2.04**	1.89	2.04	**1.80**	2.50	2.69	**2.35**
100	2.22	2.33	**2.09**	**1.99**	2.24	2.02	2.36	2.47	**2.19**
105	2.11	2.15	**1.99**	1.93	2.01	**1.91**	2.38	2.38	**2.09**
110	2.28	2.21	**2.01**	1.97	2.14	**1.89**	2.83	2.56	**2.17**
115	2.10	2.15	**1.98**	1.91	2.07	**1.88**	2.81	2.46	**2.02**
120	2.17	2.27	**1.96**	1.97	2.07	**1.89**	2.37	2.52	**2.15**
125	2.33	2.40	**2.03**	1.96	2.16	**1.92**	2.56	2.60	**2.26**
130	2.34	2.53	**2.24**	**2.23**	2.49	2.24	2.58	2.55	**2.25**
135	2.53	2.60	**2.25**	2.43	2.57	**2.38**	2.68	2.57	**2.09**
140	2.39	2.47	**2.12**	2.11	2.24	**2.05**	2.71	2.77	**2.28**
145	2.27	2.33	**2.09**	1.95	2.12	**1.94**	2.56	2.55	**2.36**
150	2.21	2.30	**2.10**	**1.91**	2.03	1.92	2.72	2.76	**2.37**
155	2.35	2.47	**2.12**	2.03	2.04	**1.92**	2.69	2.77	**2.63**
160	2.37	2.45	**2.12**	2.21	2.30	**2.04**	2.50	2.60	**2.17**
165	2.18	2.23	**2.08**	1.97	2.10	**1.93**	2.41	2.44	**2.20**
170	2.23	2.30	**2.06**	2.13	2.20	**1.92**	2.51	2.53	**2.16**
175	2.33	2.35	**2.16**	1.99	2.13	**1.89**	3.05	2.90	**2.38**
180	2.29	2.36	**2.04**	2.05	2.13	**1.93**	2.49	2.53	**2.16**

https://doi.org/10.5194/egusphere-2025-4590
Preprint. Discussion started: 6 January 2026

Table A2. Ensemble nowcasting uncertainty (in terms of RMSE dispersions, $\mathrm{RMSE}_{I_{90}}$) across 1 to 3 h forecast lead times before and after applying CSGD-adjustments (EA-ST).

Lead time (minute)	All			Summer			Winter		
	Original	CSGD-L	CSGD-NL	Original	CSGD-L	CSGD-NL	Original	CSGD-L	CSGD-NL
5	1.97	2.01	**1.77**	1.82	1.87	**1.70**	2.22	2.20	**1.86**
10	2.31	2.31	**2.11**	2.17	2.22	**2.11**	2.63	2.54	**2.04**
15	2.47	2.46	**2.21**	2.32	2.36	**2.24**	2.71	2.63	**2.10**
20	2.38	2.41	**2.15**	2.11	2.17	**1.99**	2.80	2.79	**2.42**
25	2.26	2.24	**2.02**	2.06	2.08	**1.91**	2.56	2.49	**2.16**
30	2.31	2.30	**2.06**	1.99	2.01	**1.83**	2.96	2.95	**2.49**
35	2.32	2.32	**2.10**	2.08	2.09	**1.90**	2.62	2.63	**2.35**
40	2.34	2.35	**2.09**	2.25	2.26	**2.07**	2.53	2.52	**2.09**
45	2.26	2.26	**2.07**	2.14	2.14	**1.98**	2.38	2.39	**2.17**
50	2.38	2.36	**2.08**	2.16	2.15	**1.96**	2.69	2.66	**2.29**
55	2.33	2.33	**2.06**	2.11	2.14	**1.95**	2.80	2.79	**2.28**
60	2.37	2.39	**2.10**	2.23	2.24	**1.99**	2.52	2.54	**2.23**
65	2.43	2.42	**2.15**	2.28	2.27	**2.04**	2.63	2.62	**2.29**
70	2.67	2.66	**2.38**	2.50	2.50	**2.29**	3.00	2.98	**2.53**
75	2.79	2.78	**2.51**	2.64	2.65	**2.46**	3.04	2.96	**2.53**
80	2.71	2.69	**2.43**	2.43	2.44	**2.23**	3.20	3.17	**2.78**
85	2.57	2.51	**2.27**	2.38	2.33	**2.13**	2.87	2.79	**2.44**
90	2.59	2.57	**2.32**	2.27	2.24	**2.05**	3.17	3.17	**2.77**
95	2.63	2.63	**2.36**	2.34	2.32	**2.12**	2.89	2.89	**2.67**
100	2.56	2.54	**2.32**	2.41	2.41	**2.21**	2.91	2.89	**2.46**
105	2.45	2.43	**2.21**	2.27	2.24	**2.06**	2.69	2.68	**2.36**
110	2.59	2.58	**2.29**	2.36	2.34	**2.12**	2.93	2.85	**2.54**
115	2.56	2.51	**2.26**	2.30	2.31	**2.11**	3.07	2.99	**2.54**
120	2.60	2.56	**2.26**	2.39	2.36	**2.12**	2.79	2.76	**2.44**
125	2.60	2.60	**2.32**	2.37	2.37	**2.10**	2.86	2.81	**2.56**
130	2.79	2.78	**2.47**	2.56	2.57	**2.33**	3.23	3.16	**2.70**
135	2.85	2.85	**2.62**	2.66	2.67	**2.50**	3.25	3.24	**2.81**
140	2.82	2.81	**2.50**	2.48	2.48	**2.27**	3.35	3.35	**2.95**
145	2.65	2.60	**2.35**	2.44	2.40	**2.19**	2.99	2.93	**2.53**
150	2.70	2.66	**2.44**	2.34	2.31	**2.11**	3.22	3.21	**2.89**
155	2.73	2.72	**2.47**	2.40	2.37	**2.18**	3.02	3.02	**2.79**
160	2.60	2.60	**2.38**	2.39	2.40	**2.19**	2.96	2.96	**2.67**
165	2.51	2.49	**2.28**	2.29	2.28	**2.10**	2.81	2.79	**2.50**
170	2.68	2.65	**2.38**	2.42	2.40	**2.20**	2.98	2.98	**2.67**
175	2.60	2.57	**2.33**	2.37	2.36	**2.14**	3.09	3.05	**2.65**
180	2.71	2.67	**2.38**	2.51	2.45	**2.17**	2.92	2.88	**2.63**

https://doi.org/10.5194/egusphere-2025-4590
Preprint. Discussion started: 6 January 2026

Table A3. Pearson correlation coefficients between GR and original/CSGD-adjusted deterministic nowcasts across 1 to 3 h forecast lead times (EA-ST).

Lead time (minute)	All			Summer			Winter		
	Original	CSGD-L	CSGD-NL	Original	CSGD-L	CSGD-NL	Original	CSGD-L	CSGD-NL
5	0.673	0.645	**0.685**	0.698	0.682	**0.698**	0.655	0.627	**0.675**
10	**0.702**	0.686	0.673	**0.704**	0.686	0.700	**0.704**	0.699	0.646
15	**0.646**	0.634	0.639	0.639	0.621	**0.651**	**0.654**	0.650	0.627
20	**0.613**	0.605	0.607	**0.636**	0.626	0.634	**0.587**	0.584	0.577
25	0.595	0.586	**0.598**	0.570	0.564	**0.583**	**0.630**	0.626	0.619
30	0.544	0.527	**0.553**	0.554	0.536	**0.566**	0.535	0.521	**0.540**
35	0.487	0.453	**0.503**	**0.515**	0.491	0.513	0.466	0.432	**0.495**
40	0.479	0.440	**0.490**	**0.485**	0.457	0.478	0.486	0.442	**0.509**
45	0.491	0.453	**0.497**	**0.483**	0.450	0.481	0.514	0.472	**0.523**
50	**0.471**	0.441	0.465	**0.449**	0.416	0.443	**0.499**	0.475	0.493
55	0.445	0.407	**0.450**	**0.453**	0.414	0.443	0.443	0.408	**0.459**
60	**0.439**	0.402	0.439	**0.422**	0.384	0.413	0.466	0.431	**0.470**
65	**0.402**	0.368	0.396	**0.382**	0.341	0.371	**0.429**	0.403	0.426
70	**0.385**	0.352	0.377	**0.392**	0.343	0.376	**0.383**	0.364	0.381
75	**0.412**	0.386	0.391	**0.388**	0.343	0.374	**0.438**	0.428	0.410
80	**0.385**	0.355	0.365	**0.361**	0.311	0.344	**0.411**	0.398	0.387
85	**0.408**	0.380	0.385	**0.365**	0.327	0.364	**0.460**	0.443	0.413
90	**0.379**	0.344	0.378	**0.382**	0.338	0.375	0.380	0.352	**0.384**
95	**0.359**	0.319	0.344	**0.364**	0.318	0.346	**0.357**	0.324	0.344
100	**0.339**	0.305	0.326	**0.329**	0.283	0.312	**0.356**	0.335	0.347
105	**0.366**	0.331	0.351	**0.346**	0.302	0.329	**0.397**	0.371	0.382
110	**0.331**	0.299	0.320	**0.337**	0.295	0.317	**0.334**	0.310	0.326
115	**0.327**	0.301	0.322	0.312	0.278	**0.313**	**0.346**	0.328	0.335
120	**0.329**	0.299	0.317	**0.311**	0.268	0.293	**0.354**	0.335	0.346
125	**0.282**	0.246	0.273	**0.288**	0.241	0.268	**0.286**	0.259	0.282
130	**0.286**	0.262	0.279	**0.286**	0.237	0.261	0.289	0.286	**0.298**
135	**0.277**	0.250	0.274	**0.276**	0.231	0.259	0.281	0.272	**0.292**
140	0.249	0.223	**0.252**	**0.252**	0.207	0.235	0.250	0.240	**0.272**
145	**0.279**	0.255	0.277	**0.272**	0.237	0.265	0.290	0.279	**0.292**
150	**0.296**	0.267	0.288	**0.281**	0.239	0.268	**0.312**	0.294	0.311
155	**0.282**	0.251	0.271	**0.260**	0.222	0.247	**0.307**	0.282	0.298
160	**0.254**	0.226	0.250	**0.229**	0.191	0.222	0.284	0.267	**0.286**
165	0.260	0.235	**0.264**	**0.241**	0.204	0.239	0.283	0.272	**0.295**
170	**0.254**	0.231	0.254	**0.260**	0.225	0.248	0.247	0.238	**0.261**
175	**0.260**	0.235	0.258	**0.264**	0.229	0.253	0.258	0.241	**0.264**
180	0.252	0.224	**0.254**	**0.232**	0.196	0.229	0.280	0.261	**0.288**

https://doi.org/10.5194/egusphere-2025-4590
Preprint. Discussion started: 6 January 2026

Table A4. Pearson correlation coefficients between GR and original/CSGD-adjusted ensemble nowcasts across 1 to 3 h forecast lead times (EA-ST).

Lead time (minute)	All			Summer			Winter		
	Original	CSGD-L	CSGD-NL	Original	CSGD-L	CSGD-NL	Original	CSGD-L	CSGD-NL
5	0.552	0.516	**0.589**	0.571	0.542	**0.592**	0.538	0.501	**0.588**
10	0.489	0.456	**0.533**	0.520	0.491	**0.545**	0.463	0.431	**0.521**
15	0.474	0.453	**0.510**	0.490	0.467	**0.513**	0.460	0.444	**0.507**
20	0.437	0.404	**0.459**	0.454	0.418	**0.461**	0.421	0.393	**0.456**
25	0.444	0.419	**0.475**	0.445	0.419	**0.470**	0.447	0.423	**0.482**
30	0.420	0.387	**0.459**	0.447	0.415	**0.470**	0.395	0.364	**0.446**
35	0.403	0.362	**0.428**	0.416	0.379	**0.425**	0.392	0.350	**0.431**
40	0.397	0.362	**0.417**	0.391	0.357	**0.404**	0.408	0.371	**0.433**
45	0.401	0.361	**0.416**	0.395	0.362	**0.409**	0.411	0.365	**0.425**
50	0.360	0.320	**0.377**	0.369	0.331	**0.380**	0.350	0.310	**0.372**
55	0.367	0.327	**0.376**	0.384	0.343	**0.387**	0.350	0.311	**0.361**
60	0.344	0.308	**0.354**	0.353	0.317	**0.360**	0.334	0.299	**0.345**
65	0.307	0.271	**0.321**	0.313	0.279	**0.324**	0.301	0.263	**0.317**
70	0.287	0.254	**0.301**	0.316	0.278	**0.322**	0.258	0.230	**0.277**
75	0.275	0.250	**0.293**	0.294	0.262	**0.306**	0.254	0.236	**0.276**
80	0.259	0.230	**0.267**	0.274	0.240	**0.280**	0.242	0.218	**0.252**
85	0.267	0.239	**0.283**	0.277	0.249	**0.291**	0.254	0.229	**0.270**
90	0.272	0.242	**0.278**	0.298	0.267	**0.302**	0.244	0.215	**0.249**
95	0.245	0.217	**0.257**	0.266	0.236	**0.272**	0.221	0.197	**0.237**
100	0.241	0.212	**0.248**	0.257	0.227	**0.261**	0.222	0.195	**0.230**
105	0.246	0.215	**0.253**	0.264	0.234	**0.269**	0.224	0.194	**0.230**
110	0.226	0.197	**0.234**	0.253	0.223	**0.257**	0.195	0.169	**0.204**
115	0.227	0.198	**0.233**	0.259	0.226	**0.262**	0.190	0.165	**0.195**
120	0.217	0.193	**0.224**	0.242	0.214	**0.247**	0.187	0.167	**0.193**
125	**0.202**	0.172	0.201	**0.233**	0.199	0.229	**0.164**	0.141	0.163
130	0.181	0.157	**0.186**	**0.222**	0.190	0.221	0.138	0.123	**0.146**
135	0.177	0.155	**0.185**	**0.217**	0.188	0.215	0.135	0.121	**0.149**
140	0.168	0.145	**0.172**	**0.199**	0.171	0.198	0.133	0.117	**0.140**
145	0.182	0.160	**0.187**	0.204	0.180	**0.207**	0.154	0.135	**0.157**
150	0.175	0.151	**0.180**	0.206	0.179	**0.209**	0.142	0.121	**0.146**
155	**0.167**	0.140	0.166	**0.190**	0.161	0.187	**0.139**	0.116	0.139
160	**0.170**	0.144	0.166	**0.189**	0.160	0.184	**0.144**	0.123	0.139
165	0.163	0.137	**0.166**	0.186	0.159	**0.189**	**0.133**	0.110	0.132
170	**0.152**	0.129	0.151	**0.179**	0.153	0.177	**0.120**	0.101	0.116
175	0.153	0.132	**0.154**	**0.182**	0.157	0.181	0.118	0.103	**0.119**
180	0.146	0.123	**0.152**	0.174	0.148	**0.175**	0.113	0.094	**0.117**

https://doi.org/10.5194/egusphere-2025-4590
Preprint. Discussion started: 6 January 2026

Table A5. Overall bias (OB) values between GR and original/CSGD-adjusted deterministic nowcasts across 1 to 3 h forecast lead times (EA-ST).

Lead time (minute)	All			Summer			Winter		
	Original	CSGD-L	CSGD-NL	Original	CSGD-L	CSGD-NL	Original	CSGD-L	CSGD-NL
5	**1.018**	0.736	0.723	**0.933**	0.662	0.671	1.177	**0.876**	0.822
10	**0.950**	0.688	0.673	**0.877**	0.621	0.628	**1.084**	0.811	0.756
15	**0.932**	0.681	0.667	**0.856**	0.612	0.617	**1.072**	0.811	0.761
20	**0.976**	0.715	0.697	**0.912**	0.654	0.652	**1.094**	0.827	0.780
25	**0.937**	0.692	0.674	**0.849**	0.610	0.617	**1.103**	0.846	0.783
30	**0.939**	0.696	0.682	**0.863**	0.625	0.630	**1.080**	0.825	0.777
35	**0.978**	0.728	0.708	**0.877**	0.637	0.643	1.164	**0.897**	0.829
40	**0.927**	0.693	0.674	**0.823**	0.599	0.607	**1.122**	0.869	0.801
45	**0.940**	0.704	0.687	**0.832**	0.611	0.617	1.146	**0.879**	0.819
50	**0.988**	0.741	0.721	**0.875**	0.642	0.648	1.201	**0.927**	0.859
55	**0.938**	0.709	0.689	**0.831**	0.614	0.619	1.137	**0.886**	0.819
60	**0.931**	0.706	0.681	**0.820**	0.608	0.612	1.139	**0.889**	0.810
65	**1.001**	0.759	0.735	**0.886**	0.660	0.661	1.212	**0.940**	0.871
70	**0.933**	0.709	0.684	**0.822**	0.612	0.613	1.134	**0.883**	0.813
75	**0.944**	0.721	0.695	**0.827**	0.620	0.619	1.157	**0.905**	0.834
80	**1.013**	0.778	0.743	**0.891**	0.673	0.668	1.229	**0.962**	0.877
85	**0.973**	0.749	0.715	**0.843**	0.638	0.630	1.214	**0.952**	0.873
90	**0.981**	0.754	0.721	**0.859**	0.652	0.642	1.200	**0.936**	0.864
95	**1.023**	0.787	0.756	**0.900**	0.684	0.675	1.248	**0.973**	0.903
100	**0.985**	0.756	0.729	**0.849**	0.646	0.640	1.237	**0.961**	0.893
105	**1.006**	0.770	0.742	**0.855**	0.648	0.645	1.288	**0.997**	0.924
110	**1.061**	0.812	0.782	**0.900**	0.683	0.678	1.360	1.053	**0.976**
115	**1.013**	0.774	0.744	**0.869**	0.660	0.653	1.278	**0.983**	0.913
120	**0.999**	0.765	0.734	**0.862**	0.657	0.650	1.252	**0.967**	0.891
125	**1.069**	0.821	0.785	**0.922**	0.704	0.696	1.338	**1.036**	0.947
130	**0.975**	0.743	0.718	**0.850**	0.648	0.644	1.203	**0.917**	0.853
135	**0.977**	0.745	0.719	**0.865**	0.662	0.655	1.180	**0.896**	0.836
140	**1.028**	0.786	0.759	**0.927**	0.711	0.702	1.209	**0.919**	0.859
145	**0.976**	0.744	0.722	**0.874**	0.671	0.664	1.164	**0.881**	0.831
150	**0.992**	0.760	0.733	**0.903**	0.695	0.687	1.153	**0.878**	0.816
155	**1.032**	0.790	0.761	**0.933**	0.716	0.708	1.215	**0.927**	0.859
160	**0.986**	0.756	0.726	**0.902**	0.695	0.681	1.144	**0.870**	0.812
165	**0.988**	0.756	0.729	**0.899**	0.694	0.682	1.155	**0.875**	0.817
170	**1.026**	0.788	0.762	**0.941**	0.726	0.717	1.188	**0.905**	0.846
175	**0.982**	0.754	0.730	**0.891**	0.686	0.678	1.157	**0.884**	0.827
180	**0.960**	0.735	0.711	**0.870**	0.668	0.659	**1.134**	0.865	0.809

https://doi.org/10.5194/egusphere-2025-4590
Preprint. Discussion started: 6 January 2026

Table A6. Overall bias (OB) values between GR and original/CSGD-adjusted ensemble nowcasts across 1 to 3 h forecast lead times (EA-ST).

Lead time (minute)	All			Summer			Winter		
	Original	CSGD-L	CSGD-NL	Original	CSGD-L	CSGD-NL	Original	CSGD-L	CSGD-NL
5	**1.014**	0.749	0.730	**0.943**	0.688	0.691	1.148	**0.864**	0.802
10	**0.949**	0.705	0.685	**0.887**	0.652	0.654	**1.062**	0.803	0.743
15	**0.952**	0.716	0.694	**0.891**	0.663	0.663	**1.069**	0.816	0.756
20	**0.988**	0.745	0.720	**0.928**	0.693	0.690	**1.090**	0.838	0.777
25	**0.953**	0.724	0.699	**0.900**	0.675	0.672	**1.048**	0.813	0.756
30	**0.966**	0.735	0.708	**0.910**	0.686	0.681	**1.066**	0.829	0.770
35	**1.026**	0.784	0.755	**0.966**	0.733	0.727	1.134	**0.889**	0.831
40	**0.971**	0.738	0.712	**0.910**	0.685	0.681	**1.066**	0.828	0.771
45	**0.974**	0.741	0.713	**0.909**	0.684	0.679	**1.078**	0.840	0.782
50	**1.021**	0.780	0.749	**0.957**	0.722	0.716	1.133	**0.891**	0.830
55	**0.972**	0.742	0.714	**0.906**	0.682	0.677	**1.076**	0.840	0.784
60	**0.967**	0.739	0.711	**0.897**	0.676	0.670	**1.083**	0.848	0.788
65	**1.040**	0.800	0.767	**0.969**	0.736	0.727	1.170	**0.923**	0.858
70	**0.964**	0.736	0.708	**0.893**	0.672	0.665	**1.077**	0.842	0.782
75	**0.974**	0.745	0.716	**0.903**	0.681	0.674	**1.087**	0.851	0.792
80	**1.042**	0.806	0.773	**0.970**	0.742	0.732	1.173	**0.930**	0.863
85	**1.002**	0.774	0.743	**0.929**	0.710	0.700	1.168	**0.927**	0.861
90	**1.004**	0.776	0.745	**0.940**	0.719	0.708	1.156	**0.919**	0.855
95	**1.055**	0.819	0.786	**0.986**	0.756	0.744	1.216	**0.971**	0.902
100	**1.010**	0.781	0.749	**0.937**	0.716	0.705	1.206	**0.964**	0.896
105	**1.038**	0.802	0.767	**0.965**	0.738	0.726	1.254	**1.002**	0.930
110	**1.093**	0.836	0.775	**1.029**	0.779	0.759	1.273	**1.001**	0.913
115	**1.001**	0.771	0.742	**0.928**	0.712	0.701	1.195	**0.949**	0.882
120	**0.982**	0.758	0.732	**0.915**	0.701	0.692	1.169	**0.935**	0.872
125	**1.053**	0.818	0.785	**0.993**	0.756	0.743	1.236	**0.995**	0.923
130	**0.973**	0.750	0.724	**0.907**	0.695	0.685	1.160	**0.926**	0.867
135	**0.969**	0.753	0.728	**0.944**	0.727	0.716	**1.016**	0.801	0.750
140	**1.041**	0.811	0.781	**1.023**	0.790	0.776	**1.073**	0.848	0.791
145	**0.987**	0.767	0.741	**0.959**	0.739	0.727	**1.042**	0.820	0.770
150	**1.009**	0.786	0.757	**0.986**	0.762	0.748	**1.051**	0.831	0.776
155	**1.067**	0.835	0.804	**1.035**	0.803	0.788	1.128	**0.896**	0.837
160	**1.003**	0.781	0.759	**0.973**	0.752	0.742	**1.061**	0.839	0.792
165	**1.017**	0.795	0.768	**0.981**	0.760	0.747	**1.086**	0.861	0.810
170	**1.078**	0.840	0.815	**1.039**	0.803	0.791	1.155	**0.913**	0.862
175	**1.024**	0.795	0.771	**0.986**	0.760	0.749	**1.097**	0.863	0.813
180	**1.035**	0.805	0.776	**0.988**	0.762	0.748	1.125	**0.889**	0.831

https://doi.org/10.5194/egusphere-2025-4590
Preprint. Discussion started: 6 January 2026

Appendix B: Variations in nowcast error variances: EA-ST

Figures B1 and B2 illustrates the variations in error variances of the original and CSGD-adjusted deterministic/ensemble nowcasts across 1 to 3 h forecast lead times.

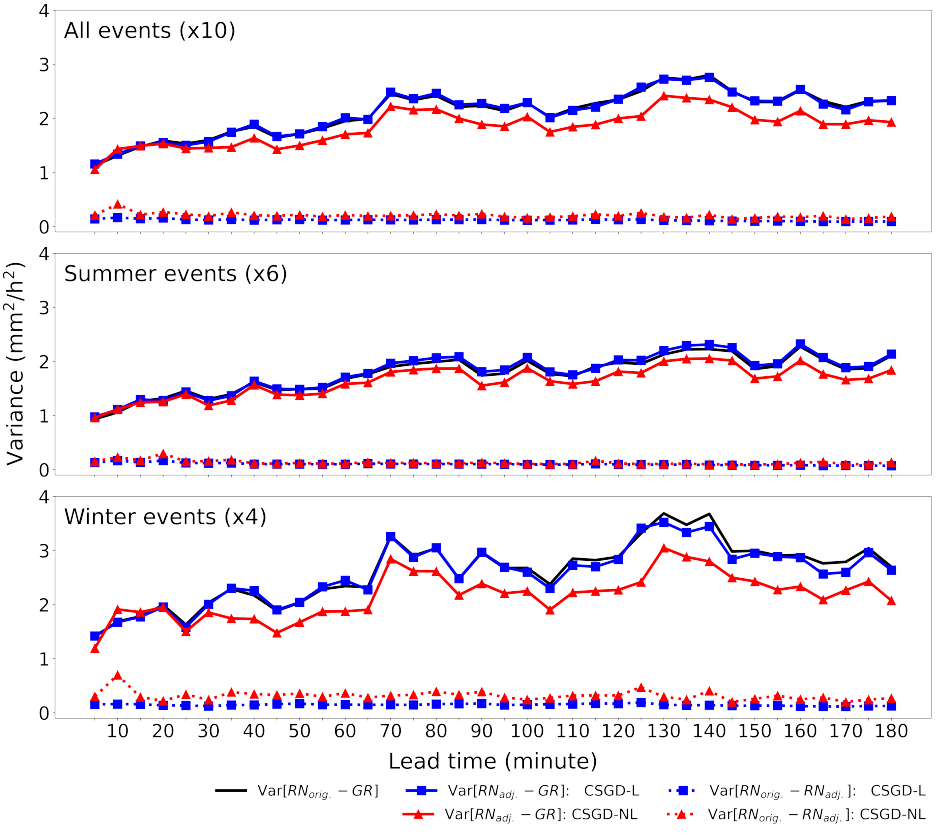

Figure B1. Error variances relative to gauge records for the original deterministic nowcasts and those adjusted using linear and non-linear CSGD models (EA-ST).

https://doi.org/10.5194/egusphere-2025-4590
Preprint. Discussion started: 6 January 2026

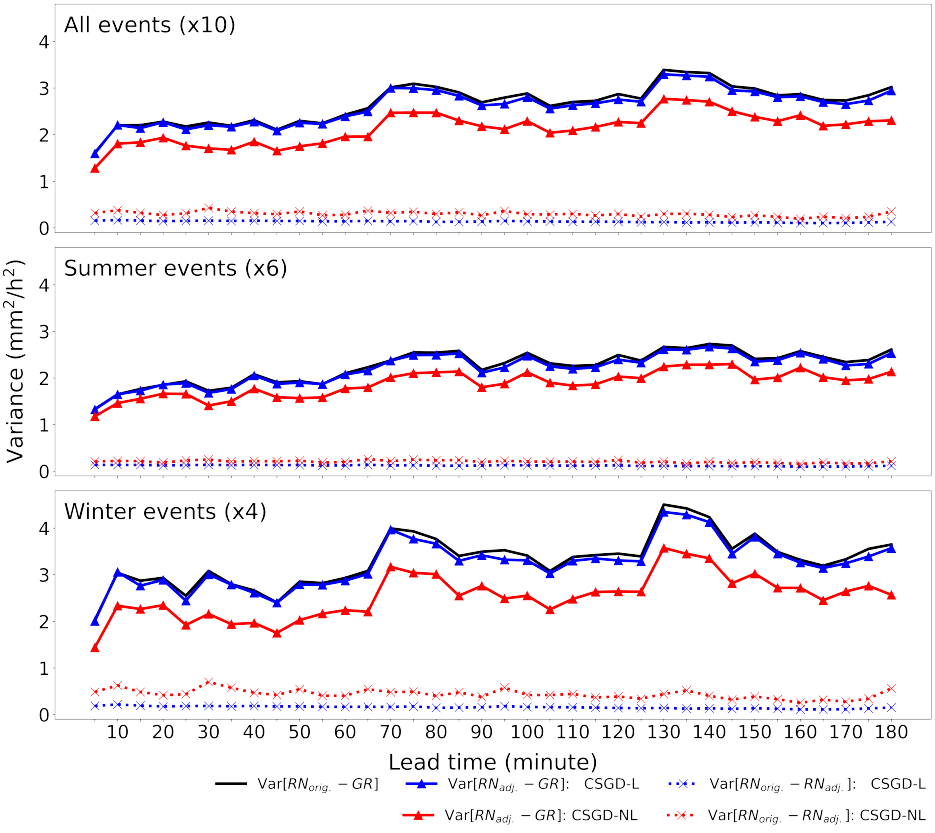

Figure B2. Error variances relative to gauge records for the original ensemble nowcasts and those adjusted using linear and non-linear CSGD models (EA-ST).

Author contributions. LW and HL jointly conceptualised research idea. HL led the model development and implementation with support from LW. LW, LH and JH co-designed the experiments to evaluate the result and prepared manuscript.

Competing interests. No competing interests are present.

Acknowledgements. The authors express their gratitude for the financial support received from three National Science and Technology Council research projects (NSTC 113-2923-M-002-001-MY4, 114-2625-M-002-011- and 114-2124-M-002-007-). In addition, the authors extend their heartfelt gratitude to Professor Daniel Wright and Dr Kaidi Peng for their invaluable technical support in working with CSGD model throughout this study.

https://doi.org/10.5194/egusphere-2025-4590
Preprint. Discussion started: 6 January 2026

References

Ayzel, G., Heistermann, M., and Winterrath, T.: Optical flow models as an open benchmark for radar-based precipitation nowcasting (rainymotion v0.1), Geosci. Model Dev., 12, 1387–1402, https://doi.org/10.5194/gmd-12-1387-2019, 2019.

Baran, S. and Nemoda, D.: Censored and shifted gamma distribution based EMOS model for probabilistic quantitative precipitation forecasting, Environmetrics, 27, 280–292, https://doi.org/10.1002/env.2391, 2016.

Beck, H. E., Zimmermann, N. E., McVicar, T. R., Vergopolan, N., Berg, A., and Wood, E. F.: Present and future Köppen-Geiger climate classification maps at 1-km resolution, Sci. Data, 5, 180 214, https://doi.org/10.1038/sdata.2018.214, 2018.

Bowler, N. E., Pierce, C. E., and Seed, A. W.: STEPS: A probabilistic precipitation forecasting scheme which merges an extrapolation nowcast with downscaled NWP, Q. J. R. Meteorol. Soc., 132, 2127–2155, https://doi.org/10.1256/qj.04.100, 2006.

Buhmann, M. D.: Radial basis functions, Acta Numer., 9, 1–38, https://doi.org/10.1017/S0962492900000015, 2000.

Cecinati, F., De Niet, A. C., Sawicka, K., and Rico-Ramirez, M. A.: Optimal temporal resolution of rainfall for urban applications and uncertainty propagation, Water, 9, 762, https://doi.org/10.3390/w9100762, 2017.

Choi, S. and Kim, Y.: Rad-cGAN v1. 0: Radar-based precipitation nowcasting model with conditional generative adversarial networks for multiple dam domains, Geosci. Model Dev., 15, 5967–5985, https://doi.org/10.5194/gmd-15-5967-2022, 2022.

Chowdhury, A., Lockart, N., Willgoose, G., Kuczera, G., Kiem, A. S., and Parana Manage, N.: Development and evaluation of a stochastic daily rainfall model with long-term variability, Hydrol. Earth Syst. Sci., 21, 6541–6558, https://doi.org/10.5194/hess-21-6541-2017, 2017.

Codo, M. and Rico-Ramirez, M. A.: Ensemble radar-based rainfall forecasts for urban hydrological applications, Geosciences, 8, 297, https://doi.org/10.3390/geoSciences8080297, 2018.

Dai, Q., Han, D., Rico-Ramirez, M. A., and Islam, T.: The impact of raindrop drift in a three-dimensional wind field on a radar–gauge rainfall comparison, Int. J. Remote Sens., 34, 7739–7760, https://doi.org/10.1080/01431161.2013.826838, 2013.

Dai, Q., Rico-Ramirez, M. A., Han, D., Islam, T., and Liguori, S.: Probabilistic radar rainfall nowcasts using empirical and theoretical uncertainty models, Hydrol. Process., 29, 66–79, https://doi.org/10.1002/hyp.10133, 2015.

Dai, Q., Yang, Q., Zhang, J., and Zhang, S.: Impact of gauge representative error on a radar rainfall uncertainty model, J. Appl. Meteorol. Climatol., 57, 2769–2787, https://doi.org/10.1175/JAMC-D-17-0272.1, 2018.

Fassnacht, S.: Estimating Alter-shielded gauge snowfall undercatch, snowpack sublimation, and blowing snow transport at six sites in the coterminous USA, Hydrol. Process., 18, 3481–3492, https://doi.org/10.1002/hyp.5806, 2004.

Germann, U., Berenguer, M., Sempere-Torres, D., and Salvade, G.: Ensemble radar precipitation estimation—A new topic on the radar horizon, in: Proceedings of the 4th European Conference on Radar in Meteorology and Hydrology (ERAD), pp. 559–562, Barcelona, Spain, 2006.

Germann, U., Berenguer, M., Sempere-Torres, D., and Zappa, M.: REAL—Ensemble radar precipitation estimation for Hydrology in a mountainous region, Q. J. R. Meteorol. Soc., 135, 445–456, https://doi.org/10.1002/qj.375, 2009.

Gires, A., Tchiguirinskaia, I., and Schertzer, D.: 3D trajectories and velocities of rainfall drops in a multifractal turbulent wind field, Atmos. Meas. Tech., 15, 5861–5875, https://doi.org/10.5194/amt-15-5861-2022, 2022.

Golding, B. W.: Nimrod: a system for generating automated very short range forecasts, Meteorol. Appl., 5, 1–16, https://doi.org/10.1017/S1350482798000577, 1998.

Gou, Y., Ma, Y., Chen, H., and Yin, J.: Utilization of a C-band polarimetric radar for severe rainfall event analysis in complex terrain over eastern China, Remote Sens., 11, 22, https://doi.org/10.3390/rs11010022, 2018.

https://doi.org/10.5194/egusphere-2025-4590
Preprint. Discussion started: 6 January 2026

Hanson, L. S. and Vogel, R.: The probability distribution of daily rainfall in the United States, in: Proceedings of the World Environmental and Water Resources Congress 2008: Ahupua'a, pp. 1–10, Honolulu, Hawaii, https://doi.org/10.1061/40976(316)585, 2008.

Harrison, D. L., Driscoll, S. J., and Kitchen, M.: Improving precipitation estimates from weather radar using quality control and correction techniques, Meteorol. Appl., 7, 135–144, https://doi.org/10.1017/S1350482700001468, 2000.

Hartke, S. H., Wright, D. B., Kirschbaum, D. B., Stanley, T. A., and Li, Z.: Incorporation of satellite precipitation uncertainty in a landslide hazard nowcasting system, J. Hydrometeorol., 21, 1741–1759, https://doi.org/10.1175/JHM-D-19-0295.1, 2020.

Huang, L., Zhang, H., Xu, P., Geng, J., Wang, C., and Liu, J.: Kriging with unknown variance components for regional ionospheric reconstruction, Sensors, 17, 468, https://doi.org/10.3390/s17030468, 2017.

Imhoff, R. O., De Cruz, L., Dewettinck, W., Brauer, C. C., Uijlenhoet, R., van Heeringen, K.-J., Velasco-Forero, C., Nerini, D., Van Ginderachter, M., and Weerts, A. H.: Scale-dependent blending of ensemble rainfall nowcasts and numerical weather prediction in the open-source pysteps library, Q. J. R. Meteorol. Soc., 149, 1335–1364, https://doi.org/10.1002/qj.4461, 2023.

Kendon, M., McCarthy, M., Jevrejeva, S., Matthews, A., Sparks, T., Garforth, J., and Kennedy, J.: State of the UK Climate 2021, Int. J. Climatol., 42, 1–80, https://doi.org/10.1002/joc.7787, 2022.

Kidd, C., Bauer, P., Turk, J., Huffman, G., Joyce, R., Hsu, K.-L., and Braithwaite, D.: Intercomparison of high-resolution precipitation products over northwest Europe, J. Hydrometeorol., 13, 67–83, https://doi.org/10.1175/JHM-D-11-042.1, 2012.

King, J. A., Engelstaedter, S., Washington, R., and Munday, C.: Variability of the Turkana low-level jet in reanalysis and models: Implications for rainfall, J. Geophys. Res. Atmos., 126, e2020JD034 154, https://doi.org/10.1029/2020JD034429, 2021.

Kuo, Y.-M., Chu, H.-J., and Pan, T.-Y.: Temporal precipitation estimation from nearby radar reflectivity using dynamic factor analysis in the mountainous Watershed–a case during Typhoon Morakot, Hydrol. Process., 28, 999–1008, https://doi.org/10.1002/hyp.9639, 2014.

Lagasio, M., Campo, L., Milelli, M., Mazzarella, V., Poletti, M. L., Silvestro, F., Ferraris, L., Federico, S., Puca, S., and Parodi, A.: SWING, the score-weighted improved nowcasting algorithm: Description and application, Water, 14, 2131, https://doi.org/10.3390/w14132131, 2022.

Levenberg, K.: A method for the solution of certain non-linear problems in least squares, Q. Appl. Math., 2, 164–168, https://doi.org/10.1090/qam/10666, 1944.

Li, Q., Wei, J., Yin, J., Qiao, Z., Cao, J., and Shi, Y.: Microphysical characteristics of raindrop size distribution and implications for radar rainfall estimation over the northeastern Tibetan Plateau, J. Geophys. Res. Atmos., 127, e2021JD035 575, https://doi.org/10.1029/2021JD035575, 2022.

Li, Z., Wright, D. B., Hartke, S. H., Kirschbaum, D. B., Khan, S., Maggioni, V., and Kirstetter, P.-E.: Toward a globally-applicable uncertainty quantification framework for satellite multisensor precipitation products based on GPM DPR, IEEE Trans. Geosci. Remote Sens., 61, 1–15, https://doi.org/10.1109/TGRS.2023.3235270, 2023.

Lin, H.-M., Wang, L.-P., and Han, J.-Y.: Gauge Rainfall Datasets from MIDAS-open (hourly) and EA-ST (5-min), Southern UK, 2016–2021, https://doi.org/10.5281/zenodo.17181918, 2025a.

Lin, H.-M., Wang, L.-P., and Han, J.-Y.: CSGD-based post-processing and verification of radar rainfall nowcasts for egusphere-2025-4590 (UK case study), https://doi.org/10.5281/zenodo.17984774, 2025b.

Liu, L., Gao, C., Zhu, Q., and Xu, Y.-P.: Evaluation of TIGGE daily accumulated precipitation forecasts over the Qu River Basin, China, J. Meteorol. Res., 33, 747–764, https://doi.org/10.1007/s13351-019-8096-z, 2019.

Lugt, D., van Hoek, M., Meirink, J. F., and van der Kooij, E.: Nowcasting for urban flash floods in Africa: a machine-learning and satellite-observation based model, in: EGU General Assembly 2021, pp. EGU21–16 002, online, 2021.

https://doi.org/10.5194/egusphere-2025-4590
Preprint. Discussion started: 6 January 2026

Maggioni, V. and Massari, C.: On the performance of satellite precipitation products in riverine flood modeling: A review, J. Hydrol., 558, 214–224, https://doi.org/10.1016/j.jhydrol.2018.01.039, 2018.

Maggioni, V., Sapiano, M. R., Adler, R. F., Tian, Y., and Huffman, G. J.: An error model for uncertainty quantification in high-time-resolution precipitation products, J. Hydrometeorol., 15, 1274–1292, https://doi.org/10.1175/JHM-D-13-0112.1, 2014.

Maggioni, V., Meyers, P. C., and Robinson, M. D.: A review of merged high-resolution satellite precipitation product accuracy during the Tropical Rainfall Measuring Mission (TRMM) era, J. Hydrometeorol., 17, 1101–1117, https://doi.org/10.1175/JHM-D-15-0190.1, 2016.

Maity, R., Dey, S., and Varun, P.: Alternative approach for estimation of precipitation using Doppler weather radar data, J. Hydrol. Eng., 20, 04015 006, https://doi.org/10.1061/(ASCE)HE.1943-5584.0001146, 2015.

Mamalakis, A., Langousis, A., Deidda, R., and Marrocu, M.: A parametric approach for simultaneous bias correction and high-resolution downscaling of climate model rainfall, Water Resour. Res., 53, 2149–2170, https://doi.org/10.1002/2016WR019578, 2017.

Massari, C. and Maggioni, V.: Error and uncertainty characterization, in: Satellite Precipitation Measurement, edited by Levizzani, V., Kidd, C., Kirschbaum, D. B., Kummerow, C. D., Nakamura, K., and Turk, F. J., vol. 69 of *Advances in Global Change Research*, pp. 515–532, Springer, Cham, https://doi.org/10.1007/978-3-030-35798-6_4, 2020.

McClean, F., Dawson, R., and Kilsby, C.: Implications of using global digital elevation models for flood risk analysis in cities, Water Resour. Res., 56, e2020WR028 241, https://doi.org/10.1029/2020WR028241, 2020.

Met Office: UK climate averages – Capel Curig, https://www.metoffice.gov.uk/research/climate/maps-and-data/uk-climate-averages/gcmnn3630, last access: 10 November 2024, a.

Met Office: Snow in the UK, https://www.metoffice.gov.uk/weather/learn-about/weather/types-of-weather/snow/snow-in-the-uk, last access: 13 June 2024, b.

Met Office: Met Office MIDAS Open: UK Land Surface Stations Data (1853–current), Centre for Environmental Data Analysis, available at: https://catalogue.ceda.ac.uk/uuid/dbd451271eb04662beade68da43546e1, last access: 27 August 2024, 2019.

Osinski, R. and Bouttier, F.: Short-range probabilistic forecasting of convective risks for aviation based on a lagged-average-forecast ensemble approach, Meteorol. Appl., 25, 105–118, https://doi.org/10.1002/met.1674, 2018.

Pan, X., Lu, Y., Zhao, K., Huang, H., Wang, M., and Chen, H.: Improving nowcasting of convective development by incorporating polarimetric radar variables into a deep-learning model, Geophys. Res. Lett., 48, e2021GL095 302, https://doi.org/10.1029/2021GL095302, 2021.

Poletti, M. L., Silvestro, F., Davolio, S., Pignone, F., and Rebora, N.: Using nowcasting technique and data assimilation in a meteorological model to improve very short range hydrological forecasts, Hydrol. Earth Syst. Sci., 23, 3823–3841, https://doi.org/10.5194/hess-23-3823-2019, 2019.

Pulkkinen, S., Nerini, D., Pérez Hortal, A. A., Velasco-Forero, C., Seed, A., Germann, U., and Foresti, L.: Pysteps: An open-source Python library for probabilistic precipitation nowcasting (v1. 0), Geosci. Model Dev., 12, 4185–4219, https://doi.org/10.5194/gmd-12-4185-2019, 2019.

Qiu, Q., Liu, J., Tian, J., Jiao, Y., Li, C., Wang, W., and Yu, F.: Evaluation of the radar QPE and rain gauge data merging methods in Northern China, Remote Sens., 12, 363, https://doi.org/10.3390/rs12030363, 2020.

Radhakrishnan, C. and Chandrasekar, V.: CASA prediction system over Dallas–Fort Worth urban network: Blending of nowcasting and high-resolution numerical weather prediction model, J. Atmos. Oceanic Technol., 37, 211–228, https://doi.org/10.1175/JTECH-D-18-0192.1, 2020.

https://doi.org/10.5194/egusphere-2025-4590
Preprint. Discussion started: 6 January 2026

Ravuri, S., Lenc, K., Willson, M., Kangin, D., Lam, R., Mirowski, P., Fitzsimons, M., Athanassiadou, M., Kashem, S., Madge, S., et al.: Skilful precipitation nowcasting using deep generative models of radar, Nature, 597, 672–677, https://doi.org/10.1038/s41586-021-03854-z, 2021.

Sandford, C.: Correcting for wind drift in high resolution radar rainfall products: a feasibility study, J. Hydrol., 531, 284–295, https://doi.org/10.1016/j.jhydrol.2015.03.023, 2015.

Schepen, A., Zhao, T., Wang, Q. J., and Robertson, D. E.: A new method for post-processing daily sub-seasonal to seasonal rainfall forecasts from GCMs and evaluation for 12 Australian catchments, Hydrol. Earth Syst. Sci. Discuss., pp. 1–27, https://doi.org/10.5194/hess-2017-380, 2017.

Schepen, A., Zhao, T., Wang, Q. J., and Robertson, D. E.: A Bayesian modelling method for post-processing daily sub-seasonal to seasonal rainfall forecasts from global climate models and evaluation for 12 Australian catchments, Hydrol. Earth Syst. Sci., 22, 1615–1628, https://doi.org/10.5194/hess-22-1615-2018, 2018.

Scheuerer, M. and Hamill, T. M.: Statistical postprocessing of ensemble precipitation forecasts by fitting censored, shifted gamma distributions, Mon. Weather Rev., 143, 4578–4596, https://doi.org/10.1175/MWR-D-15-0061.1, 2015.

Scheuerer, M. and Hamill, T. M.: Generating calibrated ensembles of physically realistic, high-resolution precipitation forecast fields based on GEFS model output, J. Hydrometeorol., 19, 1651–1670, https://doi.org/10.1175/JHM-D-18-0067.1, 2018.

Seed, A.: A dynamic and spatial scaling approach to advection forecasting, J. Appl. Meteorol. Climatol., 42, 381–388, https://doi.org/10.1175/1520-0450(2003)042<0381:ADASSA>2.0.CO;2, 2003.

Seo, B.-C. and Krajewski, W. F.: Correcting temporal sampling error in radar-rainfall: effect of advection parameters and rain storm characteristics on the correction accuracy, J. Hydrol., 531, 272–283, https://doi.org/10.1016/j.jhydrol.2015.04.018, 2015.

Shakti, P., Misumi, R., Nakatani, T., Iwanami, K., Maki, M., Seed, A. W., and Hirano, K.: Comparison of rainfall nowcasting derived from the STEPS model and JMA precipitation nowcasts, Hydrol. Res. Lett., 9, 54–60, https://doi.org/10.3178/hrl.9.54, 2015.

Shi, X., Chen, Z., Wang, H., Yeung, D.-Y., Wong, W.-K., and Woo, W.-C.: Convolutional LSTM network: a machine learning approach for precipitation nowcasting, arXiv, https://doi.org/10.48550/arXiv.1506.04214, 2015.

Shi, X., Gao, Z., Lausen, L., Wang, H., Yeung, D.-Y., Wong, W.-K., and Woo, W.-C.: Deep learning for precipitation nowcasting: a benchmark and a new model, arXiv, https://doi.org/10.48550/arXiv.1706.03458, 2017.

Sibley, A.: Analysis of the heavy orographic rainfall over North Wales, 3 and 4 February 2004, Weather, 60, 31–36, https://doi.org/10.1256/wea.155.04, 2005.

Sims, E. M. and Liu, G.: A parameterization of the probability of snow–rain transition, J. Hydrometeorol., 16, 1466–1477, https://doi.org/10.1175/JHM-D-14-0211.1, 2015.

Skripniková, K. and Řezáčová, D.: Comparison of radar-based hail detection using single-and dual-polarization, Remote Sens., 11, 1436, https://doi.org/10.3390/rs11121436, 2019.

Supajaidee, N., Chutsagulprom, N., and Moonchai, S.: An adaptive moving window kriging based on k-means clustering for spatial interpolation, Algorithms, 17, 57, https://doi.org/10.3390/a17020057, 2024.

Tahir, W., Ramli, S., Abdullah, J., Muhammad, N. S., and Rahim, N. F. H. M.: Subang Radar CAPPI Data Processing and ZR Optimization for Quantitative Precipitation Estimates (QPE) Over Langat River Basin, Jurnal Teknologi, 84, 113–122, https://doi.org/10.11113/jurnalteknologi.v84.17918, 2022.

Ten Veldhuis, J. A. E., Ochoa-Rodriguez, S., Bruni, G., Gires, A., Van Assel, J., Wang, L., Reinoso-Rodinel, R., Kroll, S., Schertzer, D., Onof, C., et al.: Weather radar for urban hydrological applications: lessons learnt and research needs identified from 4 pilot catchments in

https://doi.org/10.5194/egusphere-2025-4590
Preprint. Discussion started: 6 January 2026

North-West Europe, in: Proceedings of the 9th Weather Radar and Hydrology (WRaH) International Symposium, pp. 7–10, Washington, D.C., USA, 2014.

Villarini, G. and Krajewski, W. F.: Review of the different sources of uncertainty in single polarization radar-based estimates of rainfall, Surv. Geophys., 31, 107–129, https://doi.org/10.1007/s10712-009-9079-x, 2010.

Villarini, G., Zhang, W., Miller, P., Johnson, D. R., Grimley, L. E., and Roberts, H. J.: Probabilistic rainfall generator for tropical cyclones affecting Louisiana, Int. J. Climatol., 42, 1789–1802, https://doi.org/10.1002/joc.7335, 2022.

Wang, L.-P., Ochoa-Rodríguez, S., Van Assel, J., Pina, R. D., Pessemier, M., Kroll, S., Willems, P., and Onof, C.: Enhancement of radar rainfall estimates for urban Hydrology through optical flow temporal interpolation and Bayesian gauge-based adjustment, J. Hydrol., 531, 408–426, https://doi.org/10.1016/j.jhydrol.2015.05.049, 2015.

Wang, S. and Li, X.: Grade distribution modeling within the bauxite seams of the Wachangping mine, China, using a multi-step interpolation algorithm, Minerals, 7, 71, https://doi.org/10.3390/min7050071, 2017.

Wang, Z., Wilby, R. L., and Yu, D.: Spatial and temporal scaling of extreme rainfall in the United Kingdom, Int. J. Climatol., 44, 286–304, https://doi.org/10.1002/joc.8330, 2024.

Willems, P., De Cruz, L., Delobbe, L., Reyniers, M., Van Ootegem, L., Mahy, G., Li, X., Muñoz Lopez, C., Murlà Tuyls, D., Wang, L., et al.: PLURISK – Forecasting and management of extreme rainfall induced risks in the urban environment, Technical report, Belgian Science Policy, Brussels, 2017.

Wright, D. B., Kirschbaum, D. B., and Yatheendradas, S.: Satellite precipitation characterization, error modeling, and error correction using censored shifted gamma distributions, J. Hydrometeorol., 18, 2801–2815, https://doi.org/10.1175/JHM-D-17-0060.1, 2017.

Xi, X. and Sokolik, I. N.: Dust interannual variability and trend in Central Asia from 2000 to 2014 and their climatic linkages, J. Geophys. Res. Atmos., 120, 12–175, https://doi.org/10.1002/2015JD023228, 2015.

Xia, Q., Zhang, W., Chen, H., Lee, W.-C., Han, L., Ma, Y., and Liu, X.: Quantification of precipitation using polarimetric radar measurements during several typhoon events in Southern China, Remote Sens., 12, 2058, https://doi.org/10.3390/rs12122058, 2020.

Xu, H., Xu, K., Wang, T., and Xue, W.: Investigating flood risks of rainfall and storm tides affected by the parameter estimation coupling bivariate statistics and hydrodynamic models in the coastal city, Int. J. Environ. Res. Public Health, 19, 12 592, https://doi.org/10.3390/ijerph191912592, 2022.

Yao, S., Chen, H., Thompson, E. J., and Cifelli, R.: An improved deep learning model for high-impact weather nowcasting, IEEE J. Sel. Top. Appl. Earth Obs. Remote Sens., 15, 7400–7413, https://doi.org/10.1109/JSTARS.2022.3203398, 2022.

Ye, L., Hanson, L. S., Ding, P., Wang, D., and Vogel, R. M.: The probability distribution of daily precipitation at the point and catchment scales in the United States, Hydrol. Earth Syst. Sci., 22, 6519–6531, https://doi.org/10.5194/hess-22-6519-2018, 2018.

Yu, J., Li, X.-F., Lewis, E., Blenkinsop, S., and Fowler, H. J.: UKGrsHP: A UK high-resolution gauge–radar–satellite merged hourly precipitation analysis dataset, Clim. Dyn., 54, 2919–2940, https://doi.org/10.1007/s00382-020-05144-2, 2020.

Zhang, Y., Long, M., Chen, K., Xing, L., Jin, R., Jordan, M. I., and Wang, J.: Skilful nowcasting of extreme precipitation with NowcastNet, Nature, 619, 526–532, https://doi.org/10.1038/s41586-023-06184-4, 2023.